

## Research Article

# Modelling Friction-Induced Dynamic Instability Dedicated for Isogeometric Formulation

P. Mohanasundaram,<sup>1,2,3,4</sup> K. Shimoyama ,<sup>2,3</sup> F. Gillot ,<sup>1</sup> and S. Besset <sup>1</sup>

<sup>1</sup>LTDS, École Centrale de Lyon, Écully, France

<sup>2</sup>IFS, Tohoku University, Sendai, Japan

<sup>3</sup>ELyTMax IRL3757, CNRS, Université de Lyon, International Joint Unit, Tohoku University, Sendai, Japan

<sup>4</sup>Department of Aerospace Engineering, Tohoku University, Sendai, Japan

Correspondence should be addressed to S. Besset; [sebastien.besset@ec-lyon.fr](mailto:sebastien.besset@ec-lyon.fr)

Received 3 September 2021; Revised 13 February 2022; Accepted 4 March 2022; Published 21 November 2023

Academic Editor: Yongfang Zhang

Copyright © 2023 P. Mohanasundaram et al. This is an open access article distributed under the Creative Commons Attribution License, which permits unrestricted use, distribution, and reproduction in any medium, provided the original work is properly cited.

Flutter-type dynamic instability induced by friction is a highly nonlinear phenomenon and computationally expensive to model through transient analysis. An efficient way to make inference of such instabilities in a dynamical system is through analyzing the first-order effect of a perturbation at one of its equilibrium with eigenvalue analysis. The contact characteristics of such dynamical systems are typically modelled through the normal compliance approach with inference from experiments. In this case, the dynamical response of the system is implied to be sensitive to the contact stiffness modelled through the normal compliance approach. Typically, with the normal compliance approach, the continuum of the contact interface is approximated through a set of nonlinear springs which can be interpreted as a collocation method. Such approximations or the numerical implication of contact formulations in general for such problems is not largely studied. We focus on a variational formulation-based contact formulation without domain decomposition which is computationally efficient with small sacrifice in accuracy, where we imply that the dynamical response can be robustly modelled with the given accuracy. Further, we expose the inadequacy of the collocation method for such problems, where the dynamical system is observed to be sensitive to the extent of inaccuracy as a result of collocation for low values of contact stiffness. The inferences numerically imply the characteristics of the dynamical system for variation in contact stiffness.

## 1. Introduction

Friction naturally occurs in sliding contact. Typically, as a result of friction, the kinetic energy is largely dissipated as heat, while some of the energy is conserved as vibration which as a consequence can lead to acoustic noise [1]. The resulting noise generated by friction is more complex to model mathematically and cannot be typically explained by a single mechanism [2–4]. The complexity can be largely owed to modelling the contact interface properties and the mechanism of friction at various scales. The sound produced from friction can be purely as a result of unsteady excitation or by reaching a steady state through self-excitation [5]. Squeal noise is largely identified as the latter case, where as a

result of perturbations around equilibrium, the system reaches a new steady-state characterizing self-excitation behavior. This can be understood as coalescence of modes where two modes exist at a same frequency, leading to self-excitation between the modes under favourable conditions in the presence of friction. Even though friction is commonly associated with damping, in the case of sliding contact, it is understood that the interaction as a result of friction between the normal forces and the tangential forces relative to a contact surface gives rise to self-excitation behaviour which characterizes flutter instability. This is evident in the literature even from early analyses based on lumped models, which greatly improved the understanding of flutter-type instabilities induced by friction [6, 7].

Flutter instability induced by friction can be inferred through transient analysis with the presence of a limit cycle [8] which is nevertheless expensive to model given the nonsmooth nature of friction and to capture the high frequency characteristics over human audible range [9]. One of the most common ways to circumvent the expensive computation of such problems is through analyzing the perturbations around the equilibrium state of the dynamic problem. The equilibrium state of sliding contact problem with friction can be typically characterized as steady-sliding or quasistatic equilibrium depending on the nature of the external forces present [10, 11]. With some assumptions made over the nature of the perturbations such that the dynamics of the system for a perturbation can be expressed linearly, the system can be analysed through eigenvalue analysis. It should be noted that such linear assumptions can only characterize instabilities very close to the equilibrium. The presence of the limit cycle is inferred through complex conjugate pairs of eigenvalues  $\Re(\lambda) \pm \Im(\lambda)$  or its equivalent form  $\pm \Re(\lambda) + \Im(\lambda)$  depending on the assumed solution, and hence, such analyses are termed as complex eigenvalue analysis. A complex conjugate pair of eigenvalues only characterizes divergence from the equilibrium to reach a limit cycle but does not give any information on the actual characteristics of the limit cycle [12]. Nevertheless, CEA has been widely accepted in industrial applications such as for designing of automotive and aircraft brakes to mainly predict the presence of limit cycle which can in turn indicate the presence of squeal phenomenon and also whirl phenomenon in systems such as aircraft brakes.

Even though finite element methods are used in discretizing a complex domain, the contact interface is typically modelled through a set of linear or nonlinear springs which can be regarded as the collocation method. The sensitivity of such an approximation made over the continuum contact interface in the estimation of steady-sliding equilibrium or the prediction of instabilities through CEA is largely not studied. In this paper, we give a simple way for approximating the integrals defined over the contact interface, the variational form of contact and friction, which is similar to Gauss point to surface (GPTS) approach [13, 14] regarded as a mortar based method [15] without domain decomposition. It is intuitive that such an approximation without domain decomposition for dissimilar meshes at the contact interface is not empirically accurate. But the accuracy required depends on the quantity of interest, where in our case the sensitivity of steady-sliding equilibrium and CEA to the approximation. We focus on the variational approach without domain decomposition since it provides the best balance between computational cost and accuracy, in comparison to domain decomposition approaches which are also more complex to implement. The variational formulation is also satisfied through collocation for comparison to show the efficacy of the GPTS approach for CEA. We do not focus on the linearization part typically associated with large sliding contact problems since to compute steady-sliding equilibrium and the linearization to be made around the equilibrium for CEA requires no definition of velocity terms. We expand the definitions based on the normal compliance

approach [7, 16] where the unknown contact boundary conditions of normal stress are defined to be displacement dependent. This can be regarded as the classical mesh-tying constraint enforced through the penalty approach, where the term mesh-tying expresses the coupling of the displacement field between the domains at the contact interface. Further, we consider the isogeometric approach [17] for discretization owing to the accuracy provided in structural dynamics application [18] and contact problems [19] where the higher-order continuity of spline basis functions could be exploited [20–22].

The meaning of penalty term in classical sense is essentially to satisfy the contact constraints, where an ideal penalization is of order infinity. But in a numerical context, penalization is taken to be a high value to enforce the constraints, considering the condition number of the matrices. This could be unrealistic for a dynamical system, where the dynamical response is sensitive to stiffness at the interface which is essentially the normal compliance approach models. This is in contrast to the zero compliance model of Signorini conditions which the penalty approach essentially tries to satisfy. This means that the discretization scheme should also be accurate at lower values of penalization which could reflect the contact stiffness to be modelled with the normal compliance approach. This is because for some formulations, the accuracy of the normal stress could be improved considerably with a large value of penalization, given that the condition number of the matrices does not make it numerically unstable [19, 23]. Hence, we also focus on the accuracy of normal stress at low values of contact stiffness which is classically ignored.

We also make some inference on numerical characteristics of CEA in relation to contact stiffness and the accuracy of modelling normal stress at the contact interface, such that the sensitivity of CEA could also be implied. This is important in approximating the integrals defined over a contact domain such that it characterizes the contact interface in the interest of CEA independent or with little inference from experiments. This could be useful in applications such as optimization of systems for friction-induced dynamic instability through numerical simulations. This is mainly evident in the shape optimization of the contact interface itself [24, 25] since the contact interface has to be modelled numerically independent of experiments for a given shape variation in optimization, given the necessary experimental inference initially, parameters inferred to model normal compliance for example.

## 2. Modelling

We give a general overview of continuum formulations in this section which is useful to define the variational formulation of contact and friction, for which the discretization will be expanded in the following section. We start with the dynamical problem of contact and friction considering contact between an elastic domain and a rigid domain for the sake of simplicity §. From this, we define the steady-sliding equilibrium problem § and the problem of the dynamics of perturbation around the equilibrium §. Followed by, we

define the problem for the dynamics of perturbation explicitly  $\mathbb{S}$ , where we define explicitly the quantities of interest required to be calculated from steady-sliding equilibrium. This is to understand the approximation of the integrals defined over a contact domain for given quantities of interest which are to be defined explicitly in the interest of studying contact formulations given in  $\mathbb{S}$ . Further, for the dynamics of the perturbation problem defined explicitly, contact is considered between two elastic domains so as to give clarity in the expansion of the contact formulation in  $\mathbb{S}$ . Finally, we express the discretized form of the problems, also in matrix form for all the preceding continuum problems defined  $\mathbb{S}$ .

**2.1. Initial-Boundary Value Problem.** The initial-boundary value problem for a domain in contact with a rigid body in the presence of friction can be given as

$$\begin{aligned} \rho \ddot{\mathbf{u}} + \nabla \cdot \boldsymbol{\sigma}(\mathbf{u}) &= \mathbf{f} \text{ in } \Omega, \\ \mathbf{u} &= \mathbf{u}_D \text{ on } \Gamma_D, \end{aligned} \quad (1a)$$

$$\begin{aligned} \boldsymbol{\sigma}(\mathbf{u}) \cdot \hat{\mathbf{v}}_n &= \mathbf{t}_N \text{ on } \Gamma_N, \\ g_n &\geq 0, \sigma_n \leq 0, g_n \sigma_n = 0, \end{aligned} \quad (1b)$$

$$\begin{aligned} \|\dot{\mathbf{u}}_t\| = 0 &\implies \|\boldsymbol{\sigma}_t\| - \mu |\sigma_n| \leq 0, \\ \|\dot{\mathbf{u}}_t\| \neq 0 &\implies \boldsymbol{\sigma}_t - \mu |\sigma_n| \frac{\dot{\mathbf{u}}_t}{\|\dot{\mathbf{u}}_t\|} = 0, \end{aligned} \quad (1c)$$

on  $\Gamma_C$ ,

where  $\mathbf{u}: \Omega^3 \rightarrow \mathbb{R}^3$ ,  $\Gamma_N \cup \Gamma_D \cup \Gamma_C = \partial\Omega$ , with  $\partial\Omega$  defining the boundary of  $\Omega$ , and  $\hat{\mathbf{v}}_n$  defining the unit normal vector on  $\partial\Omega$ . Under isotropic material consideration, the constitutive equations can be defined as  $\boldsymbol{\sigma} = 2\mu_L \boldsymbol{\varepsilon} + \lambda_L \text{tr}(\boldsymbol{\varepsilon})\mathbf{I}$ , where  $\mu_L = E/2(1 + \nu)$  and  $\lambda_L = \nu E/(1 + \nu)(1 - 2\nu)$  are 3D Lamé parameters expressed in terms of Young's modulus  $E$  and Poisson's ratio  $\nu$ . The kinematic relation for the strain tensor  $\boldsymbol{\varepsilon}$  under infinitesimal displacement is defined as

$\boldsymbol{\varepsilon} = 1/2(\nabla \mathbf{u} + \nabla \mathbf{u}^T)$ . For a system with domains  $\Omega^{(a)}$  and  $\Omega^{(b)}$  in contact,  $g_n = [\mathbf{X}^{(a)} - \tilde{\mathbf{X}}^{(b)}] \cdot \hat{\mathbf{v}}_n$ , where  $\mathbf{X}$  represents the material coordinates.  $\tilde{\mathbf{X}}^{(b)}$  on  $\Omega^{(b)}$  is defined as the outward normal projection  $\hat{\mathbf{v}}_n$  from  $\partial\Omega^{(a)}$ .

Signorini conditions (1b) and Coulomb's law (1c) define elegant mathematical models for contact and friction, respectively, in macroscopic view. But such conditions have been found to lack the characteristics of contact interface in reality [7]. This leads to the view of the normal compliance approach [16] to define an approximation of the characteristics at a contact interface, also through which regularization for the multivalued mapping of (1b) can be achieved. We do not focus on the regularization of (1c) which is not useful in the scope of steady-sliding equilibrium and with the nature of the perturbations to be considered. Normal compliance is defined by  $\sigma_n$  as the function of relative normal displacement  $u_n = [\mathbf{u}^{(a)}(\mathbf{X}^{(a)}) - \mathbf{u}^{(b)}(\tilde{\mathbf{X}}^{(b)})] \cdot \hat{\mathbf{v}}_n$  (Considering  $\Omega^{(b)}$  is a rigid body,  $\mathbf{u}^{(b)} = 0$  in this case) at the interface in relation to the initial gap  $g_n$ , given as

$$-\sigma_n = c_n (u_n - g_n)_+^{m_n}, \quad (2)$$

where  $(\cdot)_+$  allows only a positive value. This can be extended to friction as

$$\begin{aligned} \|\dot{\mathbf{u}}_t\| = 0 &\implies \|\boldsymbol{\sigma}_t\| - c_t (u_n - g_n)_+^{m_t} \leq 0, \\ \|\dot{\mathbf{u}}_t\| \neq 0 &\implies \boldsymbol{\sigma}_t - c_t (u_n - g_n)_+^{m_t} \frac{\dot{\mathbf{u}}_t}{\|\dot{\mathbf{u}}_t\|} = 0, \end{aligned} \quad (3)$$

on  $\Gamma_C$ ,

where the parameters  $c_n$ ,  $m_n$ ,  $c_t$ , and  $m_t$  characterize interface properties and are to be determined from experiments. We consider the friction model purely based on Coulomb's law to focus on numerical modelling, and hence,  $c_t = \mu c_n$  and  $m_t = m_n$  in this case. With  $\Gamma_C$  known as the active set which satisfies the normal compliance constraint  $(\cdot)_+$  at a given time, the problem can be expressed as variational inequality [26], given as

$$\begin{aligned} &\int_{\Omega} \rho \ddot{\mathbf{u}} \cdot (\delta \mathbf{u} - \dot{\mathbf{u}}) d\Omega + \int_{\Omega} \boldsymbol{\sigma}(\mathbf{u}) : (\nabla \delta \mathbf{u} - \nabla \dot{\mathbf{u}}) d\Omega \\ &+ \int_{\Gamma_C} c_n (u_n - g_n)_+^{m_n} (\delta u_n - \dot{u}_n) d\Gamma_C - \int_{\Gamma_C} \mu c_n (u_n - g_n)_+^{m_n} (\|\delta \mathbf{u}_t\| - \|\dot{\mathbf{u}}_t\|) d\Gamma_C \\ &- \int_{\Gamma_N} \mathbf{t}_N \cdot (\delta \mathbf{u} - \dot{\mathbf{u}}) d\Gamma_N - \int_{\Omega} \mathbf{f} \cdot (\delta \mathbf{u} - \dot{\mathbf{u}}) d\Omega \geq 0, \end{aligned} \quad (4)$$

where  $\delta \mathbf{u}$  is the directional derivative. The solution to the above dynamical problem is often discussed in the context of nonsmooth mechanics [27, 28] which we do not focus here. But through regularization of the nondifferentiable friction functional, mainly as  $\|\dot{\mathbf{u}}_t\| \rightarrow \psi(\|\dot{\mathbf{u}}_t\|)$ , the abovementioned inequality can be expressed as variational equation [7, 11]. In this case,  $\psi$  corresponds to a continuous function over velocity for transition from stick to slip state. Given the

initial conditions  $\mathbf{u}_0$  and  $\dot{\mathbf{u}}_0$  which satisfy the inequality at the initial time, the system can be numerically integrated with time.

We focus on modelling flutter-type dynamic instability through classical theories of linear analysis, where the first-order effect of perturbations around a fixed point is analyzed. Hence, the stability of the dynamical system with frictional contact can be characterized by determining the

fixed points which are typically of quasistatic or steady-sliding equilibrium depending on the external forces and defining the dynamics for the perturbation around such fixed points. We only focus on steady-sliding equilibrium for the following discussions.

*2.2. Steady-Sliding Equilibrium.* The dynamical system can be expressed as steady-sliding equilibrium when no net acceleration is present in frictional contact. This can be seen as a series of unchanging equilibrium states with respect to time, where the equilibrium characteristics remain the same except for the relative velocity at the contact interface. Nevertheless, the problem can be expressed purely by static forces. The steady-sliding equilibrium explicitly characterizes slip condition at constant sliding velocity, and hence, at

the equilibrium,  $\sigma_t = \mu\sigma_n$  on  $\Gamma_C$ . Further, empirically, the knowledge of sliding direction  $\hat{\mathbf{v}}_k$  at any point on  $\Gamma_C$  is defined to be known a priori, and hence,  $\sigma_t = \mu\sigma_n\hat{\mathbf{v}}_k$ . This means that the nondifferential friction term of (4) as a result of the inequality (3) can be expressed as variational equation at pure slip state (The normal compliance terms in modelling  $\sigma_n$  make it nonlinear. But eventually through linearization of the normal compliance model, bilinearity could be achieved which will be discussed in the following). Since the equilibrium characteristics remain the same for all the time, the equilibrium state could be expressed with no time-dependent forces but purely by static forces. The problem of steady-sliding equilibrium can hence be expressed as

$$\int_{\Omega} \boldsymbol{\sigma}(\bar{\mathbf{u}}): \nabla \delta \mathbf{u} \, d\Omega + \underbrace{\int_{\Gamma_C} c_n (\bar{u}_n - g_n)_+^{m_n} \delta \mathbf{u} \cdot \hat{\mathbf{v}}_n \, d\Gamma_C}_{\langle \sigma_n, \delta \mathbf{u} \rangle} - \underbrace{\int_{\Gamma_C} \mu c_n (\bar{u}_n - g_n)_+^{m_n} \delta \mathbf{u} \cdot \hat{\mathbf{v}}_k \, d\Gamma_C}_{\langle \sigma_t, \delta \mathbf{u} \rangle} - \int_{\Gamma_N} \mathbf{t}_N \cdot \delta \mathbf{u} \, d\Gamma_N - \int_{\Omega} \mathbf{f} \cdot \delta \mathbf{u} \, d\Omega = 0. \quad (5)$$

The nonlinear problem can be solved through the Newton–Raphson method to obtain the steady-sliding solution  $\bar{\mathbf{u}}$ . It should be noted that for steady-sliding case with friction, nonunique solutions can exist [10, 29].

*2.3. Initial-Boundary Value Problem for Perturbation.* The perturbation of the displacement field relative to the steady-sliding equilibrium can be given as

$$\mathbf{u} = \bar{\mathbf{u}} + \tilde{\mathbf{u}}(t), \quad (6)$$

where  $\tilde{\mathbf{u}}(t)$  and  $t$  correspond to perturbed displacement field and time, respectively. The dynamics of the perturbation can be deduced by substituting  $\bar{\mathbf{u}} + \tilde{\mathbf{u}}$  in the variational equation form of (4) (The variational equation can be deduced by regularization of the nondifferentiable friction functional of the variational inequality (4). For the sake of simplicity, we do not focus on regularization since at the steady-sliding equilibrium and for perturbations around the equilibrium, the system is considered to operate beyond the discontinuity of Coulomb’s friction law, and hence, regularization has no effect) and subtracting with (5) to obtain

$$\int_{\Omega} \rho \tilde{\mathbf{u}} \cdot \delta \mathbf{u} \, d\Omega + \int_{\Omega} \boldsymbol{\sigma}(\tilde{\mathbf{u}}): \nabla \delta \mathbf{u} \, d\Omega + \int_{\Gamma_C} (c_n (\tilde{u}_n + \bar{u}_n - g_n)_+^{m_n} - c_n (\bar{u}_n - g_n)_+^{m_n}) \delta \mathbf{u} \cdot \hat{\mathbf{v}}_n \, d\Gamma_C - \int_{\Gamma_C} (\mu c_n (\tilde{u}_n + \bar{u}_n - g_n)_+^{m_n} - \mu c_n (\bar{u}_n - g_n)_+^{m_n}) \delta \mathbf{u} \cdot \hat{\mathbf{v}}_k \, d\Gamma_C = 0. \quad (7)$$

The idea is to analyze the dynamics of the system for a small perturbation such that the stability of the dynamical system can be characterized through the evolution of the dynamics for perturbation close to the steady-sliding equilibrium, where we hypothesize that the evolution of the dynamics can be sufficiently characterized linearly. This brings the question of linearizing normal compliance.

We start with the discussion of linearizing the operator  $(\cdot)_+$  under necessary conditions. The perturbation  $\tilde{u}_n$  on  $\Gamma_C$  may not result in the same active set  $\Gamma_C$ , which introduces nonlinearities defined by  $(\cdot)_+$  (Separation on  $\Gamma_C$  defines  $u_n - g_n < 0 \implies p(u_n - g_n)_+^{m_n} \longrightarrow 0$  which can only be taken into account nonlinearly. This is also true for the case contrary to separation). This can be linearized with the hypothesis that the onset of instability to model occurs close to the equilibrium  $\bar{\mathbf{u}}$  such that

the perturbation  $\tilde{\mathbf{u}}$  is small to define  $\Gamma_C$  as stationary. But this may not be true since  $\Gamma_C$  is stationary only when  $\bar{u}_n + \tilde{u}_n - g_n > 0$  (in the view of normal compliance, the perturbation  $\tilde{u}_n$  for no variation of  $\Gamma_C$  defines the variation of  $\sigma_n$ . This would have been impossible with Signorini conditions which can be regarded as the zero compliance model, where  $\tilde{u}_n > 0$  leads to strict contact separation on  $\Gamma_C$ ), implying that  $\sigma_n \ll 0$  must be true on  $\Gamma_C$  at steady-sliding equilibrium, conceivably as a result of external forces. This can lead to a new active set  $\Gamma_C$  in the current configuration  $\mathbf{X} + \bar{\mathbf{u}}(\mathbf{X})$  that satisfies  $\bar{u}_n(\mathbf{X}) + \tilde{u}_n(\mathbf{X} + \bar{\mathbf{u}}(\mathbf{X})) - g_n(\mathbf{X}) > 0$  on  $\partial\Omega$ , which depends on the nature of the perturbation  $\tilde{u}_n(\mathbf{X} + \bar{\mathbf{u}}(\mathbf{X}))$  and  $\sigma_n(\mathbf{X})$  at steady-sliding equilibrium. Perhaps, this could reveal if the linearization of the operator  $(\cdot)_+$  is realistic for a given system. To simplify, we consider  $\Gamma_C$  as stationary for the perturbation  $\tilde{\mathbf{u}}$ , which evades

the operator  $(\cdot)_+$ . With further linearization for the polynomial terms of the normal compliance, the first-order effect of the perturbation  $\tilde{\mathbf{u}}$  close to  $\bar{\mathbf{u}}$  can be expressed as

$$\begin{aligned} & (c_n(\bar{u}_n + u_n - g_n)_+^{m_n} - c_n(u_n - g_n)_+^{m_n}) \Big|_{u_n = \bar{u}_n} \\ & \approx m_n c_n (u_n - g_n)_+^{m_n - 1} \Big|_{u_n = \bar{u}_n} \tilde{u}_n. \end{aligned} \quad (8)$$

An illustration of the linearization is shown in Figure 1. It is also possible that the nonlinearity defined by the normal compliance parameters could mean that the linearization at very low values of  $\bar{u}_n - g_n$  could yield very low  $m_n c_n (\bar{u}_n - g_n)_+^{m_n - 1}$ . Hence, the assumption of stationary  $\Gamma_C$  could be justified in this case.

We provide discussions on the presumed characteristics of friction for the perturbation  $\tilde{\mathbf{u}}$  to express the dynamics of the perturbation to be linear. Even though steady equilibrium is expressed by static forces, for the perturbation  $\tilde{\mathbf{u}}(t)$ , the state of friction can change from slip state of steady-sliding equilibrium, where without regularization for friction, the dynamics of the perturbation resembles the variational inequality of equation (4). Hence, this requires further assumptions on the nature of the perturbation  $\tilde{\mathbf{u}}$  such that the system is always in slip state, which is reasonable for small perturbations and also preserves the variational equation form. For the given example, we consider contact between an elastic domain and a rigid domain, and in this case, the assumption of stationary  $\Gamma_C$  at sliding is fairly easy to consider on the elastic domain. With the dynamics considering two elastic domains in contact, for steady-sliding equilibrium, the forces at the contact interface are stationary, and hence,  $\Gamma_C$  can also be taken to be stationary even in the presence of relative motion. But for the perturbation  $\tilde{\mathbf{u}}(t)$  of such problems, the variation of forces on  $\Gamma_C$  at slip state means that the assumption of stationary  $\Gamma_C$  may not be realistic. This is true unless  $\tilde{\mathbf{u}}(t) \cdot \hat{\mathbf{v}}_k$  for the dynamical system (4) is negligibly relative to the natural frequencies of the system, which is taken to be the case here. This is evident in applications such as brake system, where the rotational frequency of brake discs is much lower than the natural frequencies of the brake system.

We define  $p(\mathbf{X}) = m_n c_n (\bar{u}_n(\mathbf{X}) - g_n(\mathbf{X}))_+^{m_n - 1}$  which can be interpreted as contact stiffness for perturbations close to steady-sliding equilibrium. For the following discussions, we do

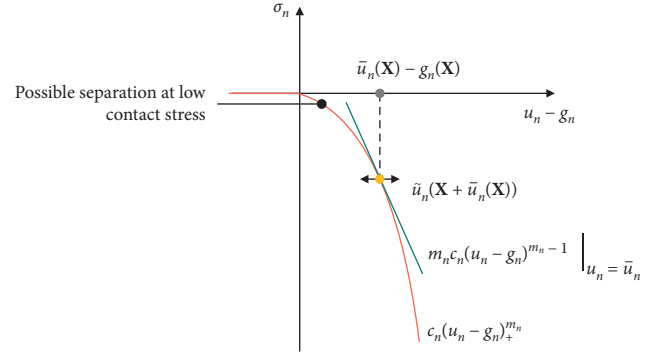


FIGURE 1: Linearization of contact defined by the normal compliance approach for the perturbation  $\tilde{\mathbf{u}}$  at the steady-sliding equilibrium  $\bar{\mathbf{u}}$ .

not relate to the experimental determination of the parameters  $c_n$  and  $m_n$ . We mainly focus on the finite element discretization of the integrals defined over  $\Gamma_C$  for the dynamics of the perturbation and the consequence of  $p(\mathbf{X})$  on the discretization schemes. Hence, the focus on the influence of discretization schemes in the estimation of steady-sliding equilibrium is not considered in this study.  $\bar{\mathbf{u}}$  effectively defines  $\Gamma_C$  at steady-sliding equilibrium, also at which normal compliance is linearized to define  $p(\mathbf{X})$ . But  $\Gamma_C$  and  $p(\mathbf{X})$  can be defined explicitly, for which a new initial-boundary value problem (9) can be considered. This is to simplify the comparison of discretization schemes for (17) with constant  $\Gamma_C$  and  $p(\mathbf{X})$ , rather than to deduce from steady-sliding equilibrium where  $\Gamma_C$  and  $p(\mathbf{X})$  could indeed vary depending on the discretization scheme.

**2.4. Initial-Boundary Value Problem for Perturbation: Explicitly Defined.** The preceding problem (1a) was expressed for contact between an elastic domain and a rigid body to simplify the expressions in focus on the nature of the problem. But to generalize the following problem for contact between elastic bodies, the subscript  $k$  is introduced to distinguish the domains in contact. With  $\Gamma_C$  and  $p(\mathbf{X})$  known a priori, either from steady-sliding equilibrium or defined explicitly, the strong form of the dynamics for  $\tilde{\mathbf{u}}$  can be expressed as

$$\begin{aligned} \rho^{(k)} \ddot{\tilde{\mathbf{u}}}^{(k)} + \nabla \cdot \boldsymbol{\sigma}^{(k)}(\tilde{\mathbf{u}}^{(k)}) &= \mathbf{0} \text{ in } \Omega^{(k)}, \\ \tilde{\mathbf{u}}^{(k)} &= \tilde{\mathbf{u}}_D^{(k)} \text{ on } \Gamma_D^{(k)}, \\ \sigma_n^{(k)}(\tilde{\mathbf{u}}^{(k)}) \hat{\mathbf{v}}_n &= -p \tilde{u}_n^{(k)} \hat{\mathbf{v}}_n, \sigma_t^{(k)}(\tilde{\mathbf{u}}^{(k)}) \hat{\mathbf{v}}_k = \mu p \tilde{u}_n^{(k)} \hat{\mathbf{v}}_k \text{ on } \Gamma_C^{(k)}. \end{aligned} \quad (9)$$

The parameters  $p(\mathbf{X})$  and  $\mu$  are defined to be constant on  $\Gamma_C$  between all the domains in contact. The variational formulation of the problem can hence be expressed as

$$\int_{\Omega^{(k)}} \rho^{(k)} \ddot{\tilde{\mathbf{u}}}^{(k)} \cdot \delta \mathbf{u}^{(k)} d\Omega^{(k)} + \int_{\Omega^{(k)}} \boldsymbol{\sigma}^{(k)}(\tilde{\mathbf{u}}^{(k)}) : \nabla \delta \mathbf{u}^{(k)} d\Omega^{(k)} - \int_{\Gamma_C^{(k)}} \mathbf{t}_C^{(k)} \cdot \delta \mathbf{u}^{(k)} d\Gamma_C^{(k)} = 0. \quad (10)$$

The traction force  $\mathbf{t}_C$  can be decomposed as

$$\int_{\Gamma_C^{(k)}} \mathbf{t}_C^{(k)} \cdot \delta \mathbf{u}^{(k)} d\Gamma_C^{(k)} = \int_{\Gamma_C^{(k)}} \sigma_n^{(k)} \hat{\mathbf{v}}_n \cdot \delta \mathbf{u}^{(k)} d\Gamma_C^{(k)} + \int_{\Gamma_C^{(k)}} \sigma_t^{(k)} \hat{\mathbf{v}}_k \cdot \delta \mathbf{u}^{(k)} d\Gamma_C^{(k)}. \quad (11)$$

Hence, with the expansion of the traction forces for  $n_k$  domains in contact, equation (10) can be expressed as

$$\sum_{k=1}^{n_k} \left\{ \int_{\Omega^{(k)}} \rho^{(k)} \tilde{\mathbf{u}}^{(k)} \cdot \delta \mathbf{u}^{(k)} d\Omega^{(k)} + \int_{\Omega^{(k)}} \boldsymbol{\sigma}^{(k)}(\tilde{\mathbf{u}}^{(k)}): \nabla \delta \mathbf{u}^{(k)} d\Omega^{(k)} = \underbrace{\int_{\Gamma_C^{(k)}} -p \tilde{u}_n^{(k)} \hat{\mathbf{v}}_n \cdot \delta \mathbf{u}^{(k)} d\Gamma_C^{(k)}}_{\langle \sigma_n^{(k)}, \delta \mathbf{u}^{(k)} \rangle_{\Gamma_C^{(k)}}} + \underbrace{\int_{\Gamma_C^{(k)}} \mu p \tilde{u}_n^{(k)} \hat{\mathbf{v}}_k \cdot \delta \mathbf{u}^{(k)} d\Gamma_C^{(k)}}_{\langle \sigma_t^{(k)}, \delta \mathbf{u}^{(k)} \rangle_{\Gamma_C^{(k)}}} \right\}. \quad (12)$$

To simplify, we consider contact between two domains  $\Omega^{(a)}$  and  $\Omega^{(b)}$ , with the derivation of traction forces on  $\Omega^{(a)}$ .

Hence, the inner products  $\langle \sigma_n^{(a)}, \delta \mathbf{u}^{(a)} \rangle_{\Gamma_C^{(a)}}$  and  $\langle \sigma_t^{(a)}, \delta \mathbf{u}^{(a)} \rangle_{\Gamma_C^{(a)}}$  can be expressed as

$$\langle \sigma_n^{(a)}, \delta \mathbf{u}^{(a)} \rangle_{\Gamma_C^{(a)}} = - \int_{\Gamma_C^{(a)}} p \tilde{u}_n^{(a)} \hat{\mathbf{v}}_n \cdot \delta \mathbf{u}^{(a)} d\Gamma_C^{(a)} = - \int_{\Gamma_C^{(a)}} p [(\tilde{\mathbf{u}}^{(a)} - \tilde{\mathbf{u}}^{(b)}) \cdot \hat{\mathbf{v}}_n] \delta \mathbf{u}^{(a)} \cdot \hat{\mathbf{v}}_n d\Gamma_C^{(a)}, \quad (13)$$

$$\langle \sigma_t^{(a)}, \delta \mathbf{u}^{(a)} \rangle_{\Gamma_C^{(a)}} = \int_{\Gamma_C^{(a)}} \mu p \tilde{u}_n^{(a)} \hat{\mathbf{v}}_n \cdot \delta \mathbf{u}^{(a)} d\Gamma_C^{(a)} = \int_{\Gamma_C^{(a)}} \mu p [(\tilde{\mathbf{u}}^{(a)} - \tilde{\mathbf{u}}^{(b)}) \cdot \hat{\mathbf{v}}_n] \delta \mathbf{u}^{(a)} \cdot \hat{\mathbf{v}}_k d\Gamma_C^{(a)}. \quad (14)$$

The traction forces on  $\Omega^{(b)}$  can similarly be defined from the conservation of momentum as  $\sigma_n^{(a)} = -\sigma_n^{(b)}$  and  $\sigma_t^{(a)} = -\sigma_t^{(b)}$ .

**2.5. Finite Element Approximation.** We introduce the function space  $\mathbf{V} := \{\delta \mathbf{u} \in (H^1(\Omega))^3 \mid \delta \mathbf{u} = \mathbf{u}_D \text{ on } \Gamma_D\}$  in which we seek the solution  $\mathbf{u}$ , where the Sobolev space  $(H^1(\Omega))^3 := \{\delta \mathbf{u} \in (L^2(\Omega))^3, \nabla \delta \mathbf{u} \in (L^2(\Omega))^3\}$  and the  $L^2$  norm:  $\|\delta \mathbf{u}\|_{L^2} = \langle \delta \mathbf{u}, \delta \mathbf{u} \rangle = \int_{\Omega} \delta \mathbf{u}^2 d\Omega < \infty$ . A subspace  $(H^{1/2}(\Gamma_C))^3$  can be defined as the restriction of  $(H^1(\Omega))^3$  on  $\Gamma_C$ , i.e.,  $\mathbf{u} \in H^1(\Omega) \rightarrow H^{1/2}(\Gamma_C)$ , defined through the normal compliance approach. Even though  $\mathbf{t}$  is typically defined to be in  $(L^2(\Omega))^3$ , the unknown a priori conditions

of  $\mathbf{t}$  on  $\Gamma_C$  imply  $\sigma_n, \sigma_t \in (H^{-1/2}(\Gamma_C))^3$ , where  $(H^{-1/2}(\Gamma_C))^3$  is the dual of the space  $(H^{1/2}(\Gamma_C))^3$ .

The solution  $\mathbf{u} \in \mathbf{V}$  can be expressed as  $\mathbf{u} = \sum_i v_i \mathbf{u}_i, \forall (v_i)^3 = \forall \mathbf{v}_i \in \mathbf{V}$ . With the finite element approach, we define a finite-dimensional function space  ${}_h \mathbf{V} \subset \mathbf{V}$ , and hence, there is some bound on  $\mathbf{v}_i \in {}_h \mathbf{V}$ . The approximation of  $\mathbf{u}$  in  ${}_h \mathbf{V}$  can be expressed as  $\mathbf{u} \approx {}_h \mathbf{u} \in {}_h \mathbf{V}$ . We focus on the definition of the space  ${}_h \mathbf{V}$  with the isogeometric approach in the next section. But in general, we give the matrix form of the variational formulations derived with  ${}_h \mathbf{V}$ .

The finite element approximation of  $\bar{\mathbf{u}} \in {}_h \mathbf{V}$  for equation (5) considering the two domains  $\Omega^{(a)}$  and  $\Omega^{(b)}$  in contact can be expressed as

$$\sum_k^{a,b} \left\{ \int_{\Omega^{(k)}} \boldsymbol{\sigma}^{(k)}({}_h \bar{\mathbf{u}}^{(k)}): \nabla \mathbf{v}_i^{(k)} d\Omega - \int_{\Gamma_C^{(k)}} \mu c_n (\bar{u}_n - {}_h g_n)_+^{m_n} \mathbf{v}_i^{(k)} \cdot \hat{\mathbf{v}}_k d\Gamma_C + \int_{\Gamma_C^{(k)}} c_n (\bar{u}_n - {}_h g_n)_+^{m_n} \mathbf{v}_i^{(k)} \cdot \hat{\mathbf{v}}_n d\Gamma_C - \int_{\Gamma_N^{(k)}} {}_h \mathbf{t}_N^{(k)} \cdot \mathbf{v}_i^{(k)} d\Gamma_N - \int_{\Omega^{(k)}} \mathbf{f}^{(k)} \cdot \mathbf{v}_i^{(k)} d\Omega = 0 \right\}, \quad \forall \mathbf{v}_i^{(k)} \in {}_h \mathbf{V}^{(k)}, \quad (15)$$

where  ${}_h g_n = [\mathbf{X}^{(k)}(\boldsymbol{\Xi}^{(k)}) - \bar{\mathbf{X}}^{(\sim k)}(\boldsymbol{\Xi}^{(\sim k)})] \cdot \hat{\mathbf{v}}_n$  and  ${}_h u_n = [{}_h \mathbf{u}^{(k)}(\mathbf{X}^{(k)}) - {}_h \mathbf{u}^{(\sim k)}(\bar{\mathbf{X}}^{(\sim k)})] \cdot \hat{\mathbf{v}}_n$ .  $\sim k$  defines the domains which are not  $k$ , i.e., in the case of contact between  $\Omega^{(a)}$  and  $\Omega^{(b)}$ ,  $k = a$

implies  $\sim k = b$  and vice-versa.  ${}_h g_n$  implies the realization of  $g_h$  with the parameterization of domains. The abovementioned expression can be expressed in the matrix form as

$$\bar{\mathbf{K}}^{(a-b)} \bar{\mathbf{U}}^{(a-b)} - \mathbf{F}_C^{(a-b)} \left( \bar{\mathbf{U}}^{(a-b)} \right) - \mathbf{F}_F^{(a-b)} \left( \bar{\mathbf{U}}^{(a-b)} \right) = \mathbf{F}, \quad (16)$$

where  $\mathbf{K}$  is the stiffness matrix,  $\mathbf{F}_C$  and  $\mathbf{F}_F$  are the nonlinear traction force vectors of contact and friction, respectively, and with  $\mathbf{F}$  being the classical force vector implying external forces. The linearization of the integrals defined over  $\Gamma_C$  in solving the steady-sliding equilibrium (5) through the

$$\sum_k^{a,b} \left\{ \int_{\Omega^{(k)}} \rho^{(k)} \ddot{\mathbf{u}}^{(k)} \cdot \mathbf{v}_i^{(k)} d\Omega^{(k)} + \int_{\Omega^{(k)}} \boldsymbol{\sigma}^{(k)}(\mathbf{u}^{(k)}): \nabla \mathbf{v}_i^{(k)} d\Omega^{(k)} + \int_{\Gamma_C^{(k)}} m_n c_n (\bar{u}_n - h g_n)^{m_n-1} \bar{u}_n \mathbf{v}_i^{(k)} \cdot \hat{\mathbf{v}}_n d\Gamma_C^{(k)} - \int_{\Gamma_C^{(k)}} \mu m_n c_n (\bar{u}_n - h g_n)^{m_n-1} \bar{u}_n \mathbf{v}_i^{(k)} \cdot \hat{\mathbf{v}}_k d\Gamma_C^{(k)} \right\} = 0, \quad \forall \mathbf{v}_i^{(k)} \in_h \mathbf{V}^{(k)}, \quad (17)$$

which can be expressed in the matrix form as

$$\mathbf{M}^{(a-b)} \ddot{\mathbf{U}}^{(a-b)} + (\mathbf{K}^{(a-b)} - \mathbf{K}_C^{(a-b)} - \mathbf{K}_F^{(a-b)}) \bar{\mathbf{U}}^{(a-b)} = 0. \quad (18)$$

The properties of the matrices can be given as follows, where  $\mathbf{M}$  and  $\mathbf{K}$  are symmetric and positive definite matrices.  $\mathbf{K}_C$  is also symmetric which essentially defines the conservation of momentum at the interface for normal contact. While  $\mathbf{K}_F$  is nonsymmetric which defines the nonconservative nature of friction at slip state. Hence, all the contact forces are expressed as displacement-dependent forces linearly. Considering a solution of the form  $\Theta e^{\lambda t}$  for  $\bar{\mathbf{U}}$ , the characteristics of the eigenvalue problem which we refer to here as CEA can be expressed as

$$(\lambda^2 \mathbf{M}^{(a-b)} + (\mathbf{K}^{(a-b)} - \mathbf{K}_C^{(a-b)} - \mathbf{K}_F^{(a-b)})) \Theta = 0. \quad (19)$$

It is evident that  $\lambda$  determines the state of the perturbed solution  $\bar{\mathbf{U}}$ . Given an eigenvalue of the form  $\lambda = \Re(\lambda) + \Im(\lambda)$ , the  $\Im(\lambda)$  part models the oscillatory behaviour while the stability of the given mode is defined by  $\Re(\lambda)$ .  $\Re(\lambda) > 0$  can be understood to characterize an unstable mode and defines the divergent nature of the solution. Similarly,  $\Re(\lambda) < 0$  can be understood to characterize a stable mode which can be interpreted as damping. The occurrence of a pair of eigenvalues  $\pm \Re(\lambda) + \Im(\lambda)$  defines the presence of a limit cycle which is of interest for applications concerning flutter-type instability induced by friction. Damping can also be factored through the definition of a matrix  $\mathbf{C}$ , typically through modal or Rayleigh damping. In the scope of modelling rotational inertia effects, gyroscopic matrix  $\mathbf{G}$  can also be defined, where  $\mathbf{C}$  and  $\mathbf{G}$  are both velocity dependent. We factor out damping and gyroscopic effects in our model to mainly focus on contact and friction modelling.

**2.6. Isogeometric Approach for Discretization of the Contact Integrals.** We define the space  ${}_h \mathbf{V}$  through the isogeometric approach to take advantage of the properties of the spline basis functions. The higher-order continuity of the spline basis functions between the knots provides superior approximation properties. The influence of the continuity in contact problems has also been largely studied for various

Newton–Raphson method takes the similar form of. This means that the tangent matrices of  $\mathbf{F}_C^{(a-b)}(\bar{\mathbf{U}}^{(a-b)})$  and  $\mathbf{F}_F^{(a-b)}(\bar{\mathbf{U}}^{(a-b)})$  to solve for  $\bar{\mathbf{U}}^{(a-b)}$  has the form  $\mathbf{K}_C^{(a-b)}$  and  $\mathbf{K}_F^{(a-b)}$ , respectively, to be discussed.

Similarly, with the substitution of equation in equation (7), for  $\bar{\mathbf{u}} \in_h \mathbf{V}$ , results in the following form:

formulations in the context of penalization or mixed formulation approach to enforce the contact constraint [19]. This is mainly true for dissimilar meshes between the domains in contact at the contact interface, where simple discretization schemes through collocation were shown to provide improved accuracy. The higher-order solution continuity is a consequence of the geometric continuity provided by spline parameterization. The geometric continuity greater than  $c^0$  is also useful to define the actual normal of the contact surface and also avoids numerical discrepancies in large displacement contact problems, as a result of the faceted  $c^0$  continuity of classical finite element meshes.

**2.7. NURBS for Approximation.** B-spline basis functions can be defined by Cox de Boor's formula as follows:

$$N_{i,0}(\xi) = \begin{cases} 1, & \xi_i \leq \xi < \xi_{i+1}, \\ 0, & \text{otherwise,} \end{cases} \quad (20)$$

$$N_{i,p}(\xi) = \frac{\xi - \xi_i}{\xi_{i+p} - \xi_i} N_{i,p-1}(\xi) + \frac{\xi_{i+p+1} - \xi}{\xi_{i+p+1} - \xi_{i+1}} N_{i+1,p-1}(\xi),$$

where  $p$  is defined recursively for  $p > 0$  to obtain a curve of degree  $p$ , which starts with a piecewise constant at  $p = 0$ . Naturally, a uniform knot vector can be defined as  $\boldsymbol{\xi} = \{\xi_1, \xi_2, \dots, \xi_{n+p+1}\}$ , where any  $\xi_i - \xi_{i+1}$  is uniformly spaced. The knot vector need not be equidistant, and the multiplicity of a knot  $\xi_i$  by  $\mathcal{M}$  in the knot vector decreases the continuity by  $c^{p-\mathcal{M}}$  across the knot  $\xi_i$ , which defines a nonuniform knot vector. Through B-spline basis functions and a knot vector  $\boldsymbol{\xi} = \{\xi_1, \dots, \xi_{n+p+1}\}$ , a B-spline curve can be defined with the basis functions and its coefficients as follows:

$$\mathbf{X}_c(\xi) = \sum_{i=1}^n N_{i,p}(\xi) \mathbf{P}_i. \quad (21)$$

The coefficients  $\mathbf{P}_i \in \mathbb{R}^d$  are the control points, with  $d$  being the dimension of the space. The definition of a weighing parameter  $w_i > 0$  associated with a respective basis

function  $N_j$ , normalized defines rational B-splines where it respects the partition of unity, given as follows:

$$\mathbf{X}_c(\xi) = \sum_{i=1}^n \frac{w_i N_{i,p}(\xi)}{\sum_{i=0}^n w_i N_{i,p}(\xi)} \mathbf{P}_i. \quad (22)$$

The parameter  $w_i$  provides a new dimension for controlling the geometry through projective transformation, while the affine transformation is achieved by  $\mathbf{P}_i$ . Hence, the combination of nonuniform knot vectors and rational basis functions defines NURBS. The higher dimensional NURBS are a natural extension of its 1-dimensional precursor through tensor product definition where the order of the tensor is the same as the dimension of the geometry. Hence, a tensor product NURBS surface can be defined as

$$\mathbf{X}_s(\xi, \eta) = \sum_{i=1}^n \sum_{j=1}^m R_{i,p}(\xi) R_{j,q}(\eta) \mathbf{P}_{i,j}, \quad (23)$$

which is supported by knot vectors  $\xi = \{\xi_1, \dots, \xi_{n+p+1}\}$  and  $\eta = \{\eta_1, \dots, \eta_{m+q+1}\}$ , for the domain  $[\xi_1, \xi_{m+q+1}] \times [\eta_1, \eta_{m+q+1}]$ , with  $n \times m$  net of control points  $\mathbf{P}_{i,j}$ . Similarly, a tensor product NURBS volume can be defined as

$$\mathbf{X}_v(\xi, \eta, \zeta) = \sum_{i=1}^n \sum_{j=1}^m \sum_{k=1}^l \frac{R_{i,p}(\xi) R_{j,q}(\eta) R_{k,r}(\zeta)}{R_{i,j,k}(\Xi)} \mathbf{P}_{i,j,k}, \quad (24)$$

where the knot vectors are given as  $\xi = \{\xi_1, \dots, \xi_{n+p+1}\}$ ,  $\eta = \{\eta_1, \dots, \eta_{m+q+1}\}$  and  $\zeta = \{\zeta_1, \dots, \zeta_{l+r+1}\}$ . The above-mentioned expression can be simply expressed in the matrix form as  $\mathbf{X}_v(\Xi) = \mathbf{R}(\Xi)\mathbf{P}$ . We also give the following notations, where to express the same degree for all the knot vectors defining a NURBS parameterization in  $\mathbb{R}^3$  is simply defined as  $\mathbb{D}^x$ , i.e.,  $(p = q = r = x): = \mathbb{D}^x$ . Similarly, for the same continuity  $y$  between the internal knots in all the knot directions is expressed as  $\mathbb{C}^y$ .

The parameterization of a domain  $\Omega \in \mathbb{R}^3$  as an initial geometric description through NURBS can be expressed as  $\tilde{\mathbf{X}}_v^{(k)}(\tilde{\Xi}^{(k)}) = \tilde{\mathbf{R}}^{(k)}(\tilde{\Xi}^{(k)})\tilde{\mathbf{P}}^{(k)}$ ,  $\mathbf{X}: \tilde{\Omega} \rightarrow \Omega$ , where  $\mathbf{X}$  defines the mapping from the parametric domain  $\tilde{\Omega}$  to the physical domain  $\Omega$ , and for simplicity, we consider the parameterization of the domain  $\Omega$  through only a single patch:  $[\xi_1, \dots, \xi_{n+p+1}] \times$

$[\eta_1, \dots, \eta_{m+q+1}] \times [\zeta_1, \dots, \zeta_{l+r+1}]$ . The analysis-suitable parameterization  $\mathbf{X}^6$  (for simplicity of the notation, we define  $\mathbf{X}$  to be the default notation for analysis-suitable parameterization of a domain  $\Omega \in \mathbb{R}^3$ ) can be achieved through the refinement of  $\tilde{\mathbf{X}} \rightarrow \mathbf{X}$  with one or several of the refinement methods:  $h$ ,  $p$ , and  $k$ , where  $\mathbf{X}$  can be defined as  $\mathbf{X}_v(\Xi) = \mathbf{R}(\Xi)\mathbf{P}$  to take into account of the modified knot vectors and control points. The isogeometric approach for the approximation of a solution is achieved through the bases  $R_{i,j,k}$ , where for the vector-valued function space  ${}_h\mathbf{V}$ , the vectorial definition of the bases  $\mathbf{R}_{i,j,k} \in \mathbb{R}^3$  can be defined as

$$\left\{ \begin{bmatrix} R_{i,j,k} \\ 0 \\ 0 \end{bmatrix} \right\} \cup \left\{ \begin{bmatrix} 0 \\ R_{i,j,k} \\ 0 \end{bmatrix} \right\} \cup \left\{ \begin{bmatrix} 0 \\ 0 \\ R_{i,j,k} \end{bmatrix} \right\}. \quad (25)$$

This can be expressed in the matrix form as  $\mathbf{R}_{i,j,k}(\Xi) = R_{i,j,k}(\Xi)\mathbb{I}$ , with  $\mathbb{I}$  being the identity matrix. Hence,

$$\mathbf{R}(\Xi) = [\mathbf{R}_{1,1,1}(\Xi) \cdots \mathbf{R}_{n,m,l}(\Xi)],$$

$$\mathbf{P} = [\mathbf{P}_{1,1,1} \cdots \mathbf{P}_{n,m,l}]^T, \mathbf{P}_{i,j,k} = [P_{i,j,k}^x \ P_{i,j,k}^y \ P_{i,j,k}^z]. \quad (26)$$

In an abstract sense, the bases  $\mathbf{R}_{i,j,k}(\Xi)$  in parametric space are transformed into the bases  $\phi_{i,j,k}(x, y, z)$  in physical space using the push-forward operator  $\circ$ , where the bases  $\phi_i$  are defined with the property  $\phi_i = \phi_{i,j,k}(\mathbf{X}) = \mathbf{R}_{i,j,k}(\Xi) \circ \mathbf{X}^{-1}$ . Hence, the approximation of a field variable on  $\Omega$  is defined through all the bases  $\phi_i$  spanning the finite-dimensional function space  $\Phi$ . For the isogeometric approach, we express the finite-dimensional space  ${}_h\mathbf{V}$  as  $\Phi$  and its associated bases  $\mathbf{v}_i$  as  $\phi_i$ . The approximation of  $\tilde{\mathbf{u}} \in \Phi$  can be defined as  ${}_h\tilde{\mathbf{u}} = \sum_{\forall i \in \Omega} \phi_i \tilde{\mathbf{u}}_i$ , expressed in the matrix form as  ${}_h\tilde{\mathbf{u}} = \mathbf{N}(\mathbf{X})\tilde{\mathbf{U}}$ , where

$$\mathbf{N}(\mathbf{X}) = [\phi_1(\mathbf{X}) \cdots \phi_{n \times m \times l}(\mathbf{X})],$$

$$\phi(\mathbf{X}) := \phi(\mathbf{X})\mathbb{I}, \quad (27)$$

$$\tilde{\mathbf{U}} = [\tilde{\mathbf{U}}_1 \cdots \tilde{\mathbf{U}}_{n \times m \times l}]^T, \tilde{\mathbf{U}}_i = [\tilde{U}_i^x \ \tilde{U}_i^y \ \tilde{U}_i^z].$$

The variational form of contact and friction given in equations (13) and (14) expressed in the function space  $\Phi$  can be defined as

$$\langle \boldsymbol{\sigma}_n^{(a)}, \phi_i^{(a)} \rangle_{\Gamma_C^{(a)}} = \int_{\Gamma_C^{(a)}} -p \left[ ({}_h\tilde{\mathbf{u}}^{(a)} - {}_h\tilde{\mathbf{u}}^{(b)}) \cdot \hat{\mathbf{v}}_n \right] \phi_i^{(a)} \cdot \hat{\mathbf{v}}_n d\Gamma_C^{(a)}, \quad \forall \phi_i^{(a)} \in \Phi^{(a)},$$

$$\langle \boldsymbol{\sigma}_t^{(a)}, \phi_i^{(a)} \rangle_{\Gamma_C^{(a)}} = \int_{\Gamma_C^{(a)}} \mu p \left[ ({}_h\tilde{\mathbf{u}}^{(a)} - {}_h\tilde{\mathbf{u}}^{(b)}) \cdot \hat{\mathbf{v}}_n \right] \phi_i^{(a)} \cdot \hat{\mathbf{v}}_n d\Gamma_C^{(a)}, \quad \forall \phi_i^{(a)} \in \Phi^{(a)}. \quad (28)$$

The expansion of the abovementioned expressions also generalizes for the definition of the tangent matrices for the nonlinear terms of contact and friction in equation (15). The parameterization of the domains  $\Omega^{(a)}$  and  $\Omega^{(b)}$  with NURBS can be expressed as  $\mathbf{X}^{(a)} = \mathbf{R}^{(a)}(\Xi^{(a)})$  and  $\mathbf{X}^{(b)} = \mathbf{R}^{(b)}(\Xi^{(b)})$ .

The active sets  $\Gamma_C^{(a)}$  and  $\Gamma_C^{(b)}$  is defined with the property  $g_n = 0$ :  $\mathbf{X}^{(a)} \cdot \hat{\mathbf{v}}_n = \tilde{\mathbf{X}}^{(b)} \cdot \hat{\mathbf{v}}_n$ , where  $\hat{\mathbf{v}}_n$  in this case is taken to be the outward normal projection from  $\Gamma_C^{(a)}$  to  $\Gamma_C^{(b)}$ . This means that  $\tilde{\mathbf{X}}^{(b)}: \tilde{\mathbf{X}}^{(b)}(\mathbf{X}^{(a)})$ , hence for  $\mathbf{X}^{(a)}$  that parametrizes  $\Gamma_C^{(a)}$ , a



projection exists that maps  $\mathbf{X}^{(a)}$  on  $\Gamma_C^{(b)}$  as  $\tilde{\mathbf{X}}^{(b)}$ . For the following explanations, we detail the derivation of traction

forces on  $\Gamma_C^{(a)}$ , which can be extended to  $\Gamma_C^{(b)}$  depending on the considered discretization scheme.

$$\begin{aligned} \langle \boldsymbol{\sigma}_n^{(a)}, \phi_i^{(a)} \rangle_{\Gamma_C^{(a)}} &= \int_{\Gamma_C^{(a)}} -p \left[ \left( \mathbf{N}^{(a)}(\mathbf{X}^{(a)}) \tilde{\mathbf{U}}^{(a)} - \mathbf{N}^{(b)}(\tilde{\mathbf{X}}^{(b)}) \tilde{\mathbf{U}}^{(b)} \right) \cdot \hat{\mathbf{v}}_n \right] \phi_i^{(a)} \cdot \hat{\mathbf{v}}_n d\Gamma_C^{(a)}, \quad \forall \phi_i^{(a)} \in \Phi^{(a)}, \\ \langle \boldsymbol{\sigma}_t^{(a)}, \phi_i^{(a)} \rangle_{\Gamma_C^{(a)}} &= \int_{\Gamma_C^{(a)}} \mu p \left[ \left( \mathbf{N}^{(a)}(\mathbf{X}^{(a)}) \tilde{\mathbf{U}}^{(a)} - \mathbf{N}^{(b)}(\tilde{\mathbf{X}}^{(b)}) \tilde{\mathbf{U}}^{(b)} \right) \cdot \hat{\mathbf{v}}_n \right] \phi_i^{(a)} \cdot \hat{\mathbf{v}}_k d\Gamma_C^{(a)}, \quad \forall \phi_i^{(a)} \in \Phi^{(a)}, \end{aligned} \quad (29)$$

were  $\hat{\mathbf{v}} := [\hat{v}^x \ \hat{v}^y \ \hat{v}^z]^T$ . Essentially, the abovementioned equations are a construct of the matrix form as

$$\int_{\Gamma_C^{(k)}} (\phi_i^{(l)} \cdot \hat{\mathbf{v}}_r) (\mathbf{N}^{(k)} \cdot \hat{\mathbf{v}}_q) d\Gamma_C^{(k)} = \int_{\Gamma_C^{(k)}} \begin{bmatrix} (\phi_1^{(k)} \cdot \hat{\mathbf{v}}_q)^T \phi_i^{(l)} \hat{v}_r^x & \dots & (\phi_{n \times m \times l}^{(k)} \cdot \hat{\mathbf{v}}_q)^T \phi_i^{(l)} \hat{v}_r^x \\ (\phi_1^{(k)} \cdot \hat{\mathbf{v}}_q)^T \phi_i^{(l)} \hat{v}_r^y & \dots & (\phi_{n \times m \times l}^{(k)} \cdot \hat{\mathbf{v}}_q)^T \phi_i^{(l)} \hat{v}_r^y \\ (\phi_1^{(k)} \cdot \hat{\mathbf{v}}_q)^T \phi_i^{(l)} \hat{v}_r^z & \dots & (\phi_{n \times m \times l}^{(k)} \cdot \hat{\mathbf{v}}_q)^T \phi_i^{(l)} \hat{v}_r^z \end{bmatrix} d\Gamma_C^{(k)}. \quad (30)$$

For  $k = l = a$ , the definition of the integrals is straight forward. In contrast, for  $k = b$  and  $l = a$ , we have terms of

the form  $\int_{\Gamma_C^{(a)}} (\phi_j^{(b)} \cdot \hat{\mathbf{v}}_q)^T \phi_i^{(a)} \hat{v}_r d\Gamma_C^{(a)}$  which can be expanded as

$$\begin{aligned} & \int_{\Gamma_C^{(a)}} \left( \phi_j^{(b)}(\tilde{\mathbf{X}}^{(b)}) \cdot \hat{\mathbf{v}}_q \right)^T \phi_i^{(a)}(\mathbf{X}^{(a)}) \hat{v}_r d\Gamma_C^{(a)} \\ &= \int_{\Gamma_C^{(a)}} \left[ \phi_j^{(b)}(\tilde{\mathbf{X}}^{(b)}) \phi_i^{(a)}(\mathbf{X}^{(a)}) \hat{v}_q^x \hat{v}_r^x \phi_j^{(b)}(\tilde{\mathbf{X}}^{(b)}) \phi_i^{(a)}(\mathbf{X}^{(a)}) \hat{v}_q^y \hat{v}_r^y \phi_j^{(b)}(\tilde{\mathbf{X}}^{(b)}) \phi_i^{(a)}(\mathbf{X}^{(a)}) \hat{v}_q^z \hat{v}_r^z \right] d\Gamma_C^{(a)}, \end{aligned} \quad (31)$$

where the integrals are simultaneously defined over the bases of the two domains in contact since  $\phi_j^{(b)} \in H^{-1/2}(\Gamma_C^{(b)})$  and  $\phi_i^{(a)} \in H^{-1/2}(\Gamma_C^{(a)})$ . Even though the definition of integral for  $\phi_j^{(b)}(\tilde{\mathbf{X}}^{(b)})$  on  $\Gamma_C^{(a)}$  exists through the projection  $\tilde{\mathbf{X}}^{(b)}(\mathbf{X}^{(a)})$ , for dissimilar meshes at the contact interface, the definition of numerical quadrature scheme for the integrals of such form requires domain decomposition to find the common span:  $(\phi_i^{(a)}(\mathbf{X}^{(a)}) \cap \phi_j^{(b)}(\tilde{\mathbf{X}}^{(b)})) : \phi_i^{(a)}(\mathbf{X}^{(a)}) \phi_j^{(b)}(\tilde{\mathbf{X}}^{(b)}) \neq 0$ .

This means that the integral exists between  $\phi_i^{(a)}(\mathbf{X}^{(a)})$  and  $\phi_j^{(b)}(\tilde{\mathbf{X}}^{(b)})$  only on the span where the projection  $\tilde{\mathbf{X}}^{(b)}(\mathbf{X}^{(a)})$  exists and hence requires a quadrature scheme specific on the span.

Inferring from the variational form of equations (29) and (30) with the expansion provided in equation (30), the following relation should hold:

$$\int_{\Gamma_C^{(a)}} \sum_{j=1}^{n \times m \times l} (\phi_j^{(a)} \cdot \hat{\mathbf{v}}_q)^T \phi_i^{(a)} \hat{v}_r d\Gamma_C^{(a)} = \int_{\Gamma_C^{(a)}} \sum_{j=1}^{n \times m \times l} (\phi_j^{(b)} \cdot \hat{\mathbf{v}}_q)^T \phi_i^{(a)} \hat{v}_r d\Gamma_C^{(a)}, \quad (32)$$

where it verifies the conservation of linear momentum at the contact interface. Since we deal with contact between flat surfaces, for the normal compliance approach which can be viewed as coupling of displacement field between the contact

surfaces, conservation of angular momentum is implicitly satisfied.

We give some intuition through the collocation approach to satisfy the conservation of momentum at the

contact interface and extend it to the definition of quadrature scheme without domain decomposition. For collocation, the integral  $\int_{\Gamma_C} \phi_i d\Gamma_C$  on one of the domains, in this case,  $\Gamma_C^{(a)}$  can be defined as  $\int_{\Gamma_C^{(a)}} \phi_i^{(a)} d\Gamma_C^{(a)} \longrightarrow \sum_{\forall i \in i^{(a)}} \phi_i^{(a)}$ , where  $i^{(a)}$  is the set of points on  $\Gamma_C^{(a)}$  which depends on the collocation scheme [21, 30]. It should be noted that this is in contrast to the collocation of the strong form. Hence, the relation (32) satisfied discretely at the collocation points takes the form as follows:

$$\sum_{j=1}^{n \times m \times l} ({}^i \phi_j^{(a)} \cdot \hat{\mathbf{v}}_q)^T {}^i \phi_i^{(a)} \hat{\mathbf{v}}_r = \sum_{j=1}^{n \times m \times l} ({}^i \phi_j^{(b)} \cdot \hat{\mathbf{v}}_q)^T {}^i \phi_i^{(a)} \hat{\mathbf{v}}_r = \phi_i^{(a)} \hat{\mathbf{v}}_r (\hat{\mathbf{v}}_q^x + \hat{\mathbf{v}}_q^y + \hat{\mathbf{v}}_q^z). \quad (34)$$

This means that any quantity defined at a collocation point  $i$  over  ${}^i \phi_i^{(a)}$  is projected equally over the bases in  $H^{-1/2}(\Gamma_C^{(a)})$  and  $H^{-1/2}(\Gamma_C^{(b)})$ . This is as a result of the properties of the NURBS basis functions similar to classical finite element basis functions which satisfy partition of unity. Since the integral is satisfied only at discrete points, the solution may not be to the necessary accuracy. The collocation strategy can be replaced by a numerical quadrature scheme as  $\int_{\Gamma_C^{(a)}} \phi_i^{(a)} d\Gamma_C^{(a)} \approx \sum_{\forall i \in i^{(a)}} {}^i w \phi_i^{(a)}$  where

$$\begin{aligned} [\mathbf{K}_C^{(a)} \mathbf{K}_C^{(a,b)}] \tilde{\mathbf{U}}^{(a-b)} &= - \sum_{\forall i \in i^{(a)}} {}^i w p \left[ ({}^i \mathbf{N}^{(a)} \cdot \hat{\mathbf{v}}_n)^T ({}^i \mathbf{N}^{(a)} \cdot \hat{\mathbf{v}}_n) ({}^i \mathbf{N}^{(a)} \cdot \hat{\mathbf{v}}_n)^T (-{}^i \mathbf{N}^{(b)} \cdot \hat{\mathbf{v}}_n) \right] \tilde{\mathbf{U}}^{(a-b)}, \\ [\mathbf{K}_F^{(a)} \mathbf{K}_F^{(a,b)}] \tilde{\mathbf{U}}^{(a-b)} &= \sum_{\forall i \in i^{(a)}} {}^i w \mu p \left[ ({}^i \mathbf{N}^{(a)} \cdot \hat{\mathbf{v}}_t)^T ({}^i \mathbf{N}^{(a)} \cdot \hat{\mathbf{v}}_n) ({}^i \mathbf{N}^{(a)} \cdot \hat{\mathbf{v}}_k)^T (-{}^i \mathbf{N}^{(b)} \cdot \hat{\mathbf{v}}_n) \right] \tilde{\mathbf{U}}^{(a-b)}, \end{aligned} \quad (35)$$

where  $\tilde{\mathbf{U}}^{(a-b)} = \begin{bmatrix} \tilde{\mathbf{U}}^{(a)} \\ \tilde{\mathbf{U}}^{(b)} \end{bmatrix}$  and  ${}^i \mathbf{N}: = [{}^i \phi_1 \ \dots \ {}^i \phi_{n \times m \times l}]$ .

$$[\mathbf{K}_C^{(a)} \mathbf{K}_C^{(a,b)}] = - \sum_{\forall i \in i^{(a)}} {}^i w p \left[ ({}^i \mathbf{R}^{(a)} \cdot \hat{\mathbf{v}}_n)^T ({}^i \mathbf{R}^{(a)} \cdot \hat{\mathbf{v}}_n) ({}^i \mathbf{R}^{(a)} \cdot \hat{\mathbf{v}}_n)^T (-{}^i \mathbf{R}^{(b)} \cdot \hat{\mathbf{v}}_n) \right] |{}^i \mathbf{J}^{(a)}|, \quad (36)$$

$$[\mathbf{K}_F^{(a)} \mathbf{K}_F^{(a,b)}] = \sum_{\forall i \in i^{(a)}} {}^i w \mu p \left[ ({}^i \mathbf{R}^{(a)} \cdot \hat{\mathbf{v}}_t)^T ({}^i \mathbf{R}^{(a)} \cdot \hat{\mathbf{v}}_n) ({}^i \mathbf{R}^{(a)} \cdot \hat{\mathbf{v}}_k)^T (-{}^i \mathbf{R}^{(b)} \cdot \hat{\mathbf{v}}_n) \right] |{}^i \mathbf{J}^{(a)}|, \quad (37)$$

where  ${}^i \mathbf{R}: = \mathbf{R}({}^i \Xi)$  and  ${}^i \Xi$  being the collocation point in the parametric space and  $\mathbf{J}$  is the Jacobian matrix for the mapping  $\Xi \longrightarrow \mathbf{X}$ .  ${}^i \Xi^{(b)}$  is the corresponding map of  $\tilde{\mathbf{X}}^{(b)}$  in the parametric space, which can be determined through the Newton-Raphson method in solving for  $\mathbf{X}^{(b)}({}^i \Xi^{(b)}) =$

$$\sum_{\forall i \in i^{(a)}} \sum_{j=1}^{n \times m \times l} ({}^i \phi_j^{(a)} \cdot \hat{\mathbf{v}}_q)^T {}^i \phi_i^{(a)} \hat{\mathbf{v}}_r = \sum_{\forall i \in i^{(a)}} \sum_{j=1}^{n \times m \times l} ({}^i \phi_j^{(b)} \cdot \hat{\mathbf{v}}_q)^T {}^i \phi_i^{(a)} \hat{\mathbf{v}}_r, \quad (33)$$

where  ${}^i \phi := {}^i \phi \ \mathbb{1}$ ,  ${}^i \phi^{(a)} := \phi^{(a)}({}^i \mathbf{X}^{(a)})$ , and  ${}^i \phi^{(b)} := \phi^{(b)}(\tilde{\mathbf{X}}^{(b)}({}^i \mathbf{X}^{(a)}))$ . This satisfies conservation of momentum at the contact interface, even though the integral  $\int_{\Gamma_C^{(a)}} \phi_i^{(a)} \phi_1^{(b)} d\Gamma_C^{(a)}$  cannot be defined accurately. For any  $i$ , the following relation holds:

${}^i \omega$ , in this case, corresponds to the quadrature points with  ${}^i \omega$  being the quadrature weights. But the notion of  ${}^i \omega$  on  $\phi^{(b)} \in H^{-1/2}(\Gamma_C^{(b)})$  may not be realistic when  ${}^i \omega$  is defined for  $\phi^{(a)} \in H^{-1/2}(\Gamma_C^{(a)})$ . This is where the higher-order continuity of the spline basis functions and increasing the number of quadrature points can be useful, which will be discussed in the next section. Hence, equations (29) and (30) approximated through a quadrature scheme can be expressed as

The integral defined over the parametric space  $\hat{\Omega}$  for the isogeometric approach takes the form.

$\tilde{\mathbf{X}}^{(b)}(\mathbf{X}^{(a)}({}^i \Xi^{(a)}))$ . Hence, there exists a mapping  ${}^i \Xi^{(a)} \longrightarrow {}^i \Xi^{(b)}$  for which  $\mathbf{X}^{(a)}({}^i \Xi^{(a)}) = \mathbf{X}^{(b)}({}^i \Xi^{(b)})$ .

From the conservation of momentum at the interface, the following relation holds  $\sigma_n^{(a)} = -\sigma_n^{(b)}$  and  $\sigma_t^{(a)} = -\sigma_t^{(b)}$ . Hence, the traction stresses on  $\Gamma_C^{(b)}$  can similarly be defined as

$$[\mathbf{K}_C^{(b,a)} \mathbf{K}_C^{(b)}] = - \sum_{\forall i \in i^{(a)}} {}^i w_P \left[ ({}^i \mathbf{R}^{(b)} \cdot \hat{\mathbf{v}}_n)^T (-{}^i \mathbf{R}^{(a)} \cdot \hat{\mathbf{v}}_n) ({}^i \mathbf{R}^{(b)} \cdot \hat{\mathbf{v}}_n)^T ({}^i \mathbf{R}^{(b)} \cdot \hat{\mathbf{v}}_n) \right] |{}^i \mathbf{J}^{(a)}|, \quad (38)$$

$$[\mathbf{K}_F^{(b,a)} \mathbf{K}_F^{(b)}] = \sum_{\forall i \in i^{(a)}} {}^i w_{\mu P} \left[ ({}^i \mathbf{R}^{(b)} \cdot \hat{\mathbf{v}}_t)^T (-{}^i \mathbf{R}^{(a)} \cdot \hat{\mathbf{v}}_n) ({}^i \mathbf{R}^{(b)} \cdot \hat{\mathbf{v}}_k)^T ({}^i \mathbf{R}^{(b)} \cdot \hat{\mathbf{v}}_n) \right] |{}^i \mathbf{J}^{(a)}|. \quad (39)$$

It should be noted that for the abovementioned equations, even though the traction forces are defined over  $\Gamma_C^{(b)}$  as  $\langle {}_h \boldsymbol{\sigma}^{(b)}, \boldsymbol{\phi}_i^{(b)} \rangle_{\Gamma^{(b)}}$ , the quadrature points' set  $i^{(a)}$  is determined only on  $\Gamma_C^{(a)}$ , where its corresponding projection on  $\Gamma_C^{(b)}$  is defined through the projection  $\tilde{\mathbf{X}}^{(b)}$ . This also includes Jacobian  $|{}^i \mathbf{J}^{(a)}|$  which is evaluated only on  $\Gamma_C^{(a)}$ , similar to equations (36) and (37). This greatly simplifies the finite element discretization of the integrals which may otherwise require the domain decomposition approach to satisfy the integrals exactly, where this as a consequence can have an effect on accuracy which is discussed in §. With the abovementioned definitions, the matrices  $\mathbf{K}_C^{(a-b)}$  and  $\mathbf{K}_F^{(a-b)}$  for the system take the form.

$$\mathbf{K}_C^{(a-b)} = \begin{bmatrix} \mathbf{K}_C^{(a)} & \mathbf{K}_C^{(a,b)} \\ \mathbf{K}_C^{(b,a)} & \mathbf{K}_C^{(b)} \end{bmatrix}, \quad (40)$$

$$\mathbf{K}_F^{(a-b)} = \begin{bmatrix} \mathbf{K}_F^{(a)} & \mathbf{K}_F^{(a,b)} \\ \mathbf{K}_F^{(b,a)} & \mathbf{K}_F^{(b)} \end{bmatrix}.$$

Since the quadrature rule or collocation is defined with respect to only one surface, it is commonly termed as half-pass. The role of  $\Gamma_C^{(a)}$  and  $\Gamma_C^{(b)}$  can be switched, and the average over the two half-pass can be taken into account to define the so called full-pass [31]. A variation of the full-pass approach is also given in [32] based on surface potentials.

Considering equation (30) given in the general form, the submatrices of the form  $\mathbf{K}_C^{(\cdot)}$  and  $\mathbf{K}_F^{(\cdot)}$ , in contrast to the form  $\mathbf{K}_C^{(a-b)}$  and  $\mathbf{K}_F^{(a-b)}$ , respectively, correspond to the case  $k = l$ . With the relation  $\sum_{j=1}^{n \times m \times l} ({}^i \phi_j^{(k)} \cdot \hat{\mathbf{v}}_q)^T {}^i \phi_i^{(l=k)} \hat{\mathbf{v}}_r = \phi_i^{(l=k)} \hat{\mathbf{v}}_r (\hat{\mathbf{v}}_q^x + \hat{\mathbf{v}}_q^y + \hat{\mathbf{v}}_q^z)$  inferred from (34),  $\mathbf{K}_C^{(\cdot)}$  and  $\mathbf{K}_F^{(\cdot)}$  can be lumped. Hence, with equation (30) for  $l = k$ , lumping can be achieved by defining  $\phi_j^{(k)} \equiv \delta_{i,j}$ ,  $\delta_{i,j}$  being the Kronecker delta product, where the inner product  $\langle \phi_j^{(k)}, \phi_i^{(l=k)} \rangle$  is expressed with the property.

$$\phi_j^{(k)} \phi_i^{(l=k)} \hat{\mathbf{v}}_r \hat{\mathbf{v}}_q = \begin{cases} \phi_i^{(l=k)} \hat{\mathbf{v}}_r \hat{\mathbf{v}}_q, & \text{if } j = i, \\ 0, & \text{if } j \neq i, \end{cases} \quad (41)$$

$l \neq k$  defines the matrices of the form  $\mathbf{K}_C^{(\cdot)}$  and  $\mathbf{K}_F^{(\cdot)}$ , where the relation  $\sum_{j=1}^{n \times m \times l} ({}^i \phi_j^{(k)} \cdot \hat{\mathbf{v}}_q)^T \phi_i^{(l \neq k)} \hat{\mathbf{v}}_r = \phi_i^{(k)} \hat{\mathbf{v}}_r (\hat{\mathbf{v}}_q^x + \hat{\mathbf{v}}_q^y + \hat{\mathbf{v}}_q^z)$  inferred from (34) holds. This preserves the conservation of momentum at the interface.

Collocation can be achieved with the weak form considering  ${}^i w = 1$ ,  $|{}^i \mathbf{J}| = 1$ , and  $i \in \mathbf{I}$  being a suitable set of collocation points for equations (36)–(39). It should be noted that for collocation schemes based on the variational

form, the effect of the area for a collocation point can be taken into account through  ${}^i w$  and  $|{}^i \mathbf{J}|$  to improve the accuracy [30]. It should be noted that as with the classical collocation method, collocation with the strong form can also be considered, where the strong form of contact and friction boundary conditions are considered, as in equation (9), which is shown to provide more accuracy for the basis functions with higher-order continuity. For the isogeometric approach, Greville and Botella points are of interest which exploit the properties of NURBS. Also, for a given NURBS parameterization, the number of Greville and Botella points is fixed which is in contrast to the Gauss quadrature scheme which can be defined independent of the NURBS parameterization. Nevertheless, the main interest with the collocation scheme is the reduction of computational cost associated with the reduced number of evaluations, where the number of Greville or Botella points is typically very low in comparison to the number of quadrature points for a reasonable accuracy. We only consider Greville points in the following section. Greville abscissae in a direction are the average of the knots in the knot vector for the direction. Further, the Greville points lie on the surface which makes it useful to define the projection  $\tilde{\mathbf{X}}$ , and the number of Greville points is the same as the number of control points.

### 3. Results and Discussion

The variational formulation satisfied through collocation with Greville points is simply termed as the collocation method, unless otherwise specified. For the following discussions, we use the term variational formulation to specify the use of quadrature scheme in an approximate sense as discussed in the preceding section, as it preserves the integral sense of the variational formulation. The results are shown with only half-pass formulation. It should be noted that the results implied with half-pass for a given formulation cannot be extended to full-pass. Since even if the patch test could be passed, it does not guarantee conditions for LBB stable [33] or the implications in CEA. Hence, for a given formulation, the full pass must be tested to imply its stability in CEA which is not considered.  $\mathbb{D}^x$  and  $\mathbb{C}^y$  are considered to be the same for all the domains in a given analysis. For the variational formulation, we define the number of Gauss abscissae between the knot spans in a direction to be the same as the order of the NURBS in that direction, unless otherwise specified. The results are mainly focused on the accuracy of the formulations inferred through a contact patch test, and the inferences are related to the sensitivity of CEA for a given formulation. Even though we only focus on the accuracy of  $\sigma_n$  through the considered contact patch test, it should be

noted that  $\sigma_t$  for steady-sliding equilibrium is given by the relation  $|\sigma_t| = \mu|\sigma_n|$ . Hence, the accuracy of  $\sigma_n$  will have a subsequent effect on  $\sigma_t$ , though the sensitivity of  $\sigma_n$  and  $\sigma_t$  on steady-sliding equilibrium is not considered in this study. Further, all the results of CEA are obtained with  $\mu = 0.7$ . To proceed with the following discussions, we introduce the global contact stiffness  $P$  at the interface  $\Gamma_C$  as  $P = \int_{\Gamma_C} p(\mathbf{X}) \, d\Gamma_C$ . Hence, a given  $P$  is constant at the interface, and the local contact stiffness  $p(\mathbf{X})$  varies depending on the accuracy of the formulations.

For the contact patch test, we consider  $p(\mathbf{X})$  to be constant on  $\Gamma_C$ , and hence, an ideal discretization should yield  $p(\mathbf{X}) = P/\text{Area}(\Gamma_C)$ . But for a given  $P$ , the local contact stiffness  $p(\mathbf{X})$  can vary depending on the approximation in obtaining a formulation. The discretization of  $p(\mathbf{X})$  has direct influence on contact normal stress  $\sigma_n$  through which the accuracy of a discretization scheme can be inferred to some extent since for some formulations, the accuracy depends on the condition number of the matrices where higher accuracy can be attained with a large value of  $P$ . For this reason, we focus on considerably low values of  $P$  in the interest of the normal compliance approach. The setting for the contact patch test is shown in Figure 2, where we consider two cuboid domains in contact with two different meshes visible through the knot vectors of the NURBS parameterization. The bottom face of  $\Omega^{(b)}$  is fixed, while the top face of  $\Omega^{(a)}$  is applied a uniform pressure of  $1000 \text{ N/m}^2$  and constrained to move normal to  $\Gamma_C^{(b)}$ . The material parameters  $E = 10^5$  and  $\nu = 0$  are defined to be the same for both the domains. Analytically, one can infer that  $|\sigma_n| = 1000 \text{ N/m}^2$  on  $\Gamma_C$ , which provides good benchmark to compare  $\sigma_n$  calculated with different formulations. The contact patch test can be defined by considering equation (15) for  $\mu = 0$  and  $\hat{\mathbf{v}}_k = 0$ . With further simplification of  $c_n = p(\mathbf{X})$  and  $m_n = 1$ , the matrix form of the problem can be solved for  $\bar{\mathbf{K}}^{(a-b)} \bar{\mathbf{U}}^{(a-b)} - \mathbf{F}_C^{(a-b)} (\bar{\mathbf{U}}^{(a-b)}) = \mathbf{F}$ . Given  $\Gamma_C^{(a)}$  and  $\Gamma_C^{(b)}$  known a priori, for  $m_n = 1$ ,  $\mathbf{F}_C^{(a-b)} (\bar{\mathbf{U}}^{(a-b)})$  can be expressed as  $\mathbf{K}_C^{(a-b)} \bar{\mathbf{U}}^{(a-b)}$ .

To begin with, we show the comparison of variational formulation with lumping and without lumping in Figure 3. Surprisingly, the approach with lumping has reduced oscillation of  $\sigma_n$  for a given  $P$ , where for the higher value of  $P = 10^{14}$ , the approach even passes the contact patch test to machine precision. For CEA 19, we consider a simple disc-pad system which can give rise to dynamic instability induced by friction. Similar to the contact patch test,  $p(\mathbf{X})$  is defined explicitly to be constant on  $\Gamma_C$ , as discussed in §. This is because  $p(\mathbf{X})$  determined through steady-sliding equilibrium can vary depending on the discretization scheme to define an unbiased comparison of CEA results. Even though the lumped approach is observed to be superior in the patch test, it proves to be numerically unstable for CEA, shown in Figures 4 and 5. We define the following notations  $\mathbf{u}^{(d)}$  and  $\mathbf{u}^{(p)}$  to express the displacement field of the disc and the pad, respectively. Even though the scale of the displacement field has no sense for the computed eigenvectors, comparison can be made relatively with the displacement field for a given eigenvector. It should be noted that we deal with complex

eigenvectors where the imaginary part of an eigenvector characterizes phase difference of the displacement field, which will not be considered here. The mode shapes in Figure 4 considered for comparison are chosen to be close in frequency and has the same characteristics in relation to the mode shape of the disc. For the lumped approach, it can be observed that the relative displacement at the contact interface of the disc is much lower in relation to the displacement field elsewhere. The arrow on which  $\mathbf{u}^{(d)} \cdot \mathbf{v}_n^{(d)}$  is plotted also traverses the boundary of the contact interface  $\partial\Gamma_C^{(d)}$  (Boundary of the contact interface can be defined as  $\partial\Gamma_C$  for the contact interface  $\Gamma_C$ ) where strong solution gradient for  $\mathbf{u}^{(d)} \cdot \mathbf{v}_n^{(d)}$  can be observed. This is in contrast to the approach without lumping where  $\mathbf{u}^{(d)} \cdot \mathbf{v}_n^{(d)}$  is smooth across  $\partial\Gamma_C^{(d)}$ . In this case, the dynamic response of the approach with lumping and without lumping is observed to be different as shown with the results in Figure 6 where the natural frequencies  $\Im(\lambda)$  and its corresponding instabilities  $\Re(\lambda)$  largely do not coincide. Empirically, the behaviour observed at the contact interface for the lumped approach seems unrealistic since  $\Gamma_C^{(d)}$  and  $\Gamma_C^{(p)}$  are observed to be locked with each other relative to the rest of the domains in contact. This could also be a consequence of the properties of NURBS basis functions and hence can be verified with classical finite element basis functions, which is not considered here. It should be noted that the role of mesh refinement at  $\partial\Gamma_C^{(d)}$  plays an important role in capturing the solution gradient since the higher-order continuity of the spline basis functions will have strong propensity to define a smooth solution across  $\partial\Gamma_C^{(d)}$ . In our case, multipatch parameterization of disc is considered where one of the patches consist of  $\Gamma_C^{(d)}$ . Hence, across  $\partial\Gamma_C^{(d)}$ ,  $h$ -refinement was achieved in the patch that contains  $\Gamma_C^{(d)}$  such that the knots can trace along side  $\partial\Gamma_C^{(p)}$  and on  $\partial\Gamma_C^{(p)}$ . But for more complicated shape of  $\partial\Gamma_C^{(p)}$ , strategies based on RBQ [34], or in the scope of local refinement T-splines [35] or THB splines [36] have to be considered. For the lack of understanding of the numerical implication with lumping, we only focus on the approach without lumping for the following discussions. Nevertheless, the above discussions reveal that the contact patch test cannot be purely accounted for the accuracy in CEA.

As it can be inferred from the contact patch test in Figure 3, the accuracy of  $\sigma_n$  can be improved with increase in  $P$ . For the contact problems defined by static analysis, when the contact constraint is satisfied with the penalty approach, it is necessary that  $p$  is large where in an ideal case  $p \rightarrow \infty$ . But for dynamical systems, contact stiffness models the interface properties which have influence on the resulting dynamical response. It has been observed that the value of contact stiffness in this case is not typically higher than the penalty value typically used in satisfying the contact constraint [37]. In this case, the variational formulation with higher-order continuity and increased number of Gauss quadrature points can yield better results. The necessary accuracy indeed depends on the sensitivity of the approximation in estimating the steady-sliding equilibrium, the effect it has on linearization for CEA, and the evaluation of  $\Re(\lambda)$  and  $\Im(\lambda)$  with CEA. In the interest of computational cost, as the order of continuity  $C^{x-1}$  is increased ( $k$

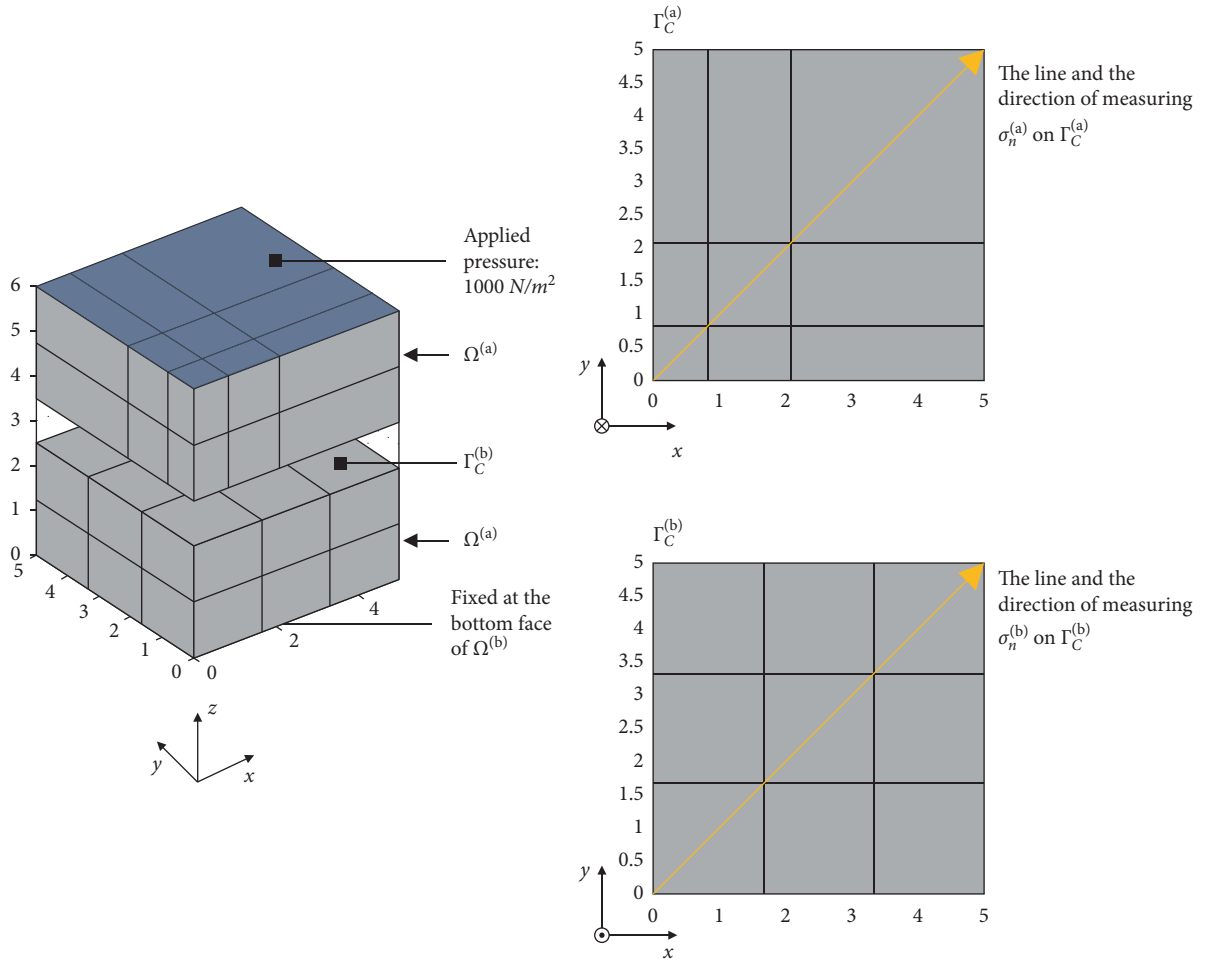


FIGURE 2: Description of the contact patch test.

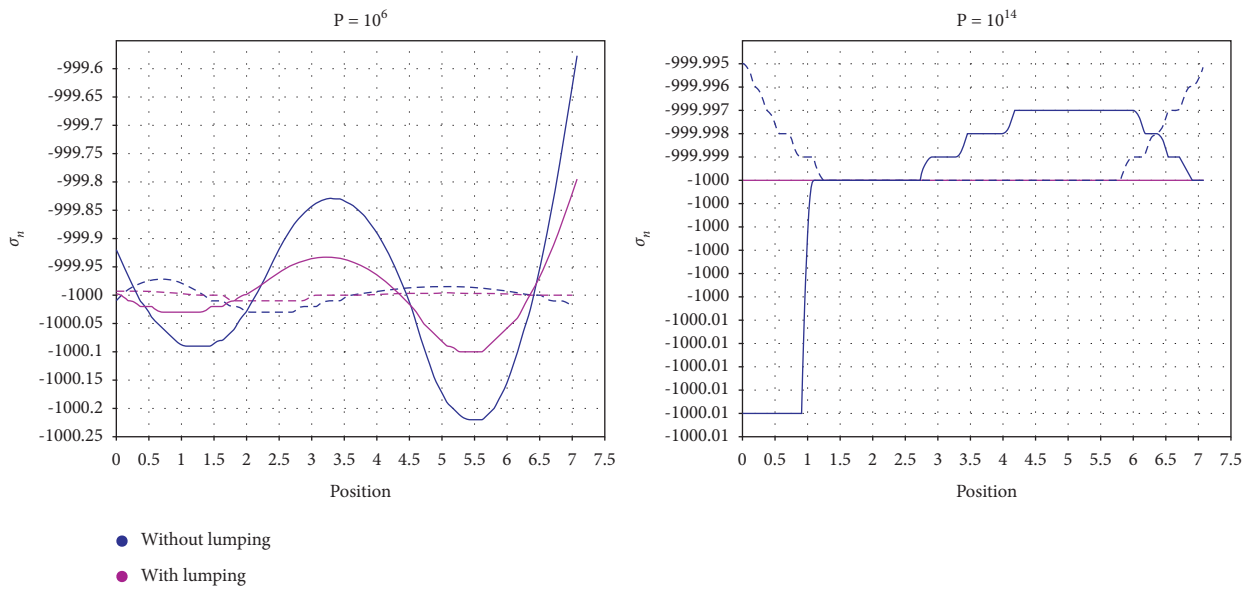


FIGURE 3: Results from the contact patch test. NURBS parameterization:  $\mathbb{D}^2\mathbb{C}^1$ ; quadrature points:  $25 \times 25$  in a knot span  $\in \mathbb{R}^2$ ; solid line:  $\sigma_n^{(b)}$  and dashed line:  $\sigma_n^{(a)}$ .

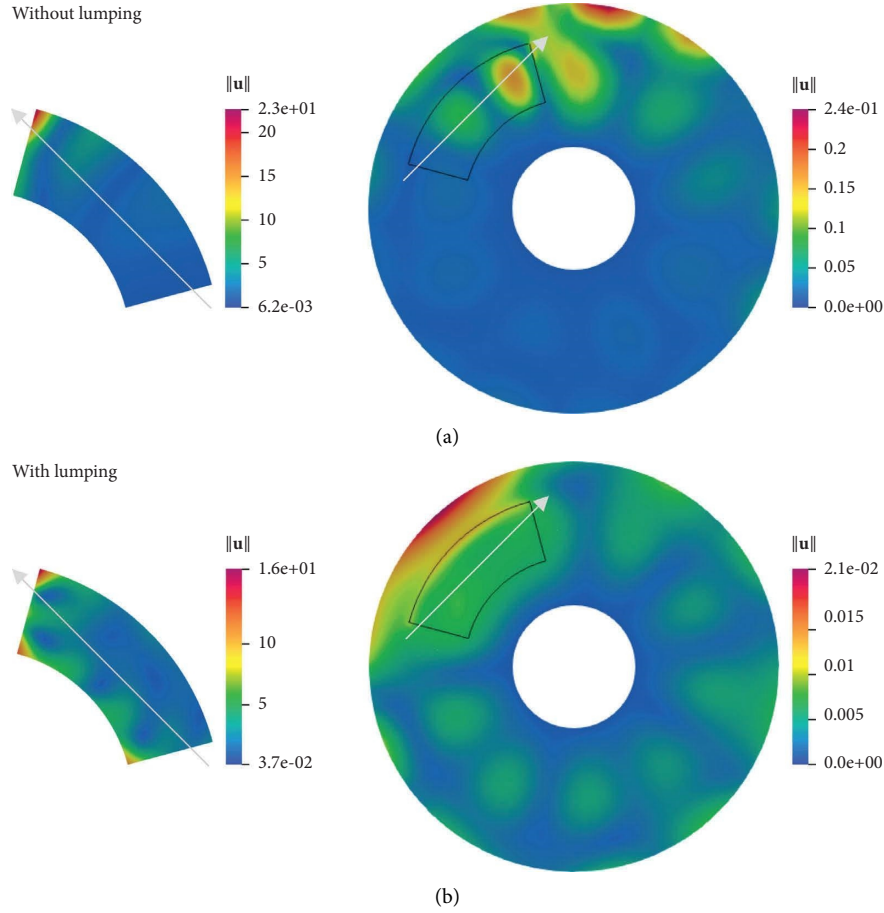


FIGURE 4: Mode shapes from CEA.  $\mathbf{u}, \hat{\mathbf{v}}_n$  is measured along the arrow, shown in Figure 5.  $P = 10^6$ ; NURBS parameterization:  $\mathbb{D}^2\mathbb{C}^1$ .

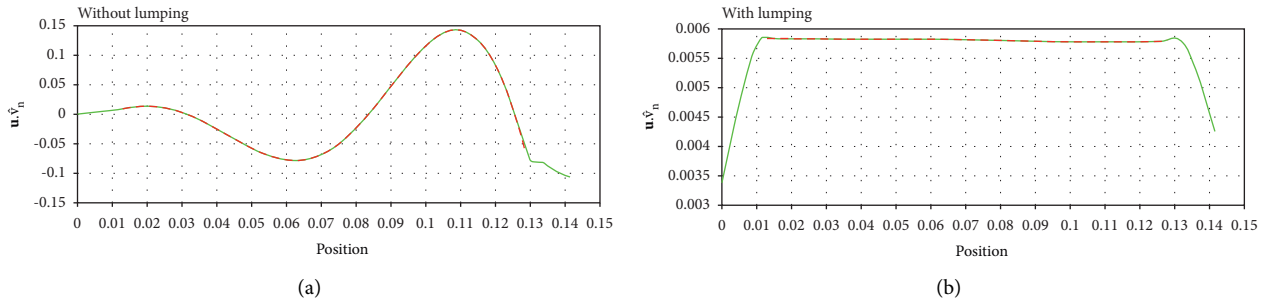


FIGURE 5: Displacement plot inferred along the arrow for the mode shapes in Figure 4. Solid line:  $\mathbf{u}^{(d)}, \mathbf{v}_n^{(d)}$  and dashed line:  $\mathbf{u}^{(p)}, \mathbf{v}_n^{(p)}$ .

refinement) with increase in degree  $\mathbb{D}^x$  ( $p$  refinement), the increase in the number of control points is of very low order. Even though the increase in the degrees of freedom of the finite element matrices is small for simultaneous  $p$  and  $k$  refinement, this can reduce the sparsity of the matrices and hence can increase the computational cost in terms of both memory and time. Hence,  $\mathbb{C}^{x-1}$  can be considered only up to a reasonable value of  $\mathbb{D}^x$  depending on the required accuracy.

With the following results, we analyze the significance of the higher-order continuity of the spline basis functions and number of Gauss quadrature points on the accuracy of  $\sigma_n$ .

The influence of the higher-order continuity is shown in Figure 7 for various  $\mathbb{D}^x$  and  $\mathbb{C}^y$  considering  $P = 10^6$ . It can be observed that the oscillation in  $\sigma_n$  decreases with increase in continuity. This can be clearly seen with comparing the cases of  $\mathbb{D}^2\mathbb{C}^0$  and  $\mathbb{D}^2\mathbb{C}^1$  defined with equal number of Gauss points between the knot spans  $\in \mathbb{R}^2$  (span  $\in \mathbb{R}^2: [\xi_i, \xi_{i+1}] \times [\eta_j, \eta_{j+1}]$ , considering that  $\Gamma_C$  is defined on the surface parameterized by knot vectors  $\xi$  and  $\eta$ ), where  $\mathbb{D}^2\mathbb{C}^1$  shows reduced oscillation of  $\sigma_n$ . While for  $\mathbb{D}^2\mathbb{C}^0$ , the solution is observed to be only  $c^0$  continuous at the knots. The results of  $\mathbb{D}^2\mathbb{C}^0$  and  $\mathbb{D}^2\mathbb{C}^1$  are shown in comparison to  $\mathbb{D}^4\mathbb{C}^3$  for which the oscillation of  $\sigma_n$  is negligible. The accuracy of  $\sigma_n$  can be

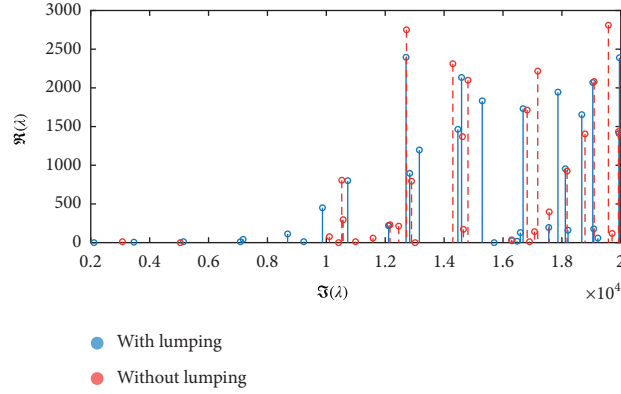


FIGURE 6: Comparison of results from CEA.  $P = 10^9$ ; NURBS parameterization:  $\mathbb{D}^2\mathbb{C}^1$ .

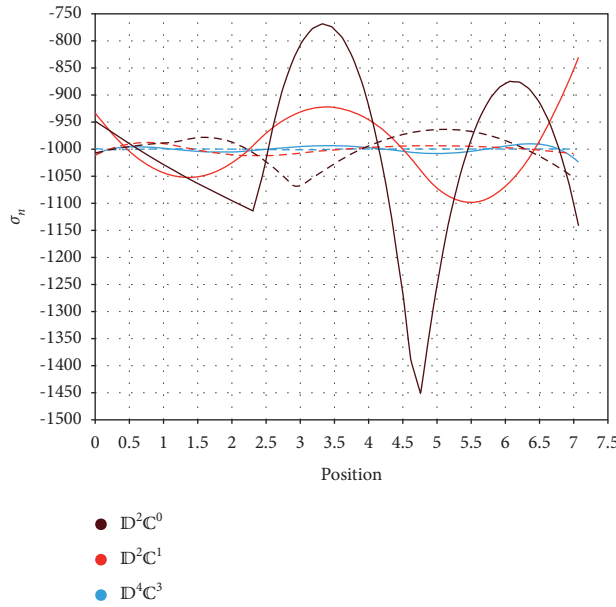


FIGURE 7: Results from the contact patch test.  $P = 10^6$ ; solid line:  $\sigma_n^{(b)}$  and dashed line:  $\sigma_n^{(a)}$ .

improved with increasing the number of Gauss quadrature points, which is shown in Figure 8. For the case of  $\mathbb{D}^4\mathbb{C}^3$  in Figure 9, the number of Gauss points is also increased with the degree by default as specified before, and hence, the addition of Gauss points also contributed to increase in accuracy along with the contribution from higher-order continuity. Nevertheless, even  $\mathbb{D}^4\mathbb{C}^3$  does not satisfy the contact patch test at  $P = 10^6$ , shown in Figure 9. It can be inferred that even though the accuracy of  $\sigma_n$  increases profoundly with initial refinement of continuity and increasing the number of Gauss quadrature points, after a certain order of continuity and number of Gauss points, the accuracy can only get up to a certain digit. Hence, from the asymptotic convergence of  $\sigma_n$  for increase in continuity and number of Gauss points, it can be inferred that the contact patch test cannot be passed to machine precision.

It can also be observed that the oscillation of  $\sigma_n^{(b)}$  is greater than  $\sigma_n^{(a)}$  for  $\mathbb{D}^x\mathbb{C}^y$ . This can be hypothesized as resulting from the quadrature scheme defined only over

$\Gamma_C^{(a)}$ , i.e., the quadrature points, Jacobian, and the quadrature weights are evaluated only on  $\Gamma_C^{(a)}$ , while only their corresponding projection is defined over  $\Gamma_C^{(b)}$ . Finally, we provide some intuition for possibly why the accuracy improves with increase in continuity and number of quadrature points for the variational formulation. As discussed in the preceding section, the approximation of the integrals defined over  $\Gamma_C$  is simplified with considering the quadrature scheme on only one of the domains in contact, while its projection is defined on the other. This is not very intuitive since the quadrature quantities such as quadrature weights  $^i w$  and the determinant of Jacobian  $^i |J|$  of the quadrature points  $i \in \mathbf{I}$  are evaluated in relation to only one of the contact domains, in this case  $\Gamma_C^{(a)}$ . Nevertheless, the projection on to  $\Gamma_C^{(b)}$  will preserve conservation of momentum at the interface. When the domain to be projected on  $\Gamma_C^{(b)}$  is  $\mathbb{C}^0$ ,  $^i w$  and  $^i |J|$  evaluated over  $\Gamma_C^{(a)}$  and projected on to a knot span  $\in \mathbb{R}^2$  parameterizing  $\Gamma_C^{(b)}$  are confined within the

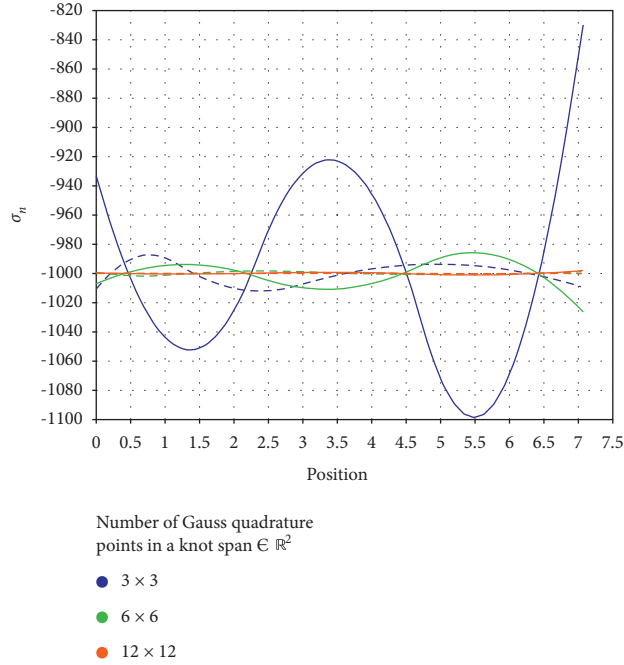


FIGURE 8: Results from the contact patch test.  $P = 10^6$ ; NURBS parameterization:  $\mathbb{D}^2\mathbb{C}^1$ ; solid line:  $\sigma_n^{(b)}$  and dashed line:  $\sigma_n^{(a)}$ .

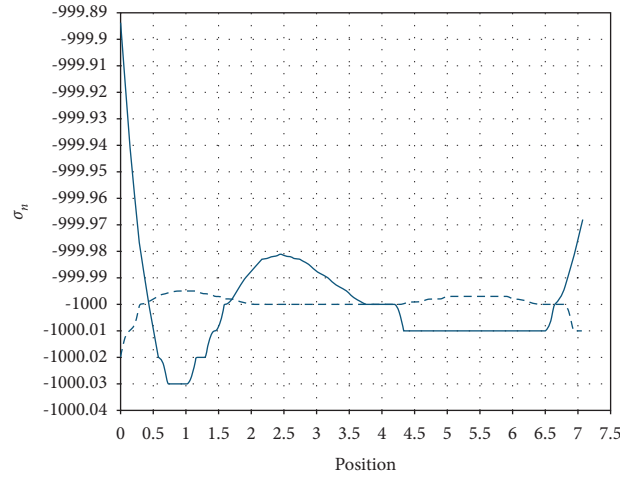


FIGURE 9: Results from the contact patch test.  $P = 10^6$ ; NURBS parameterization:  $\mathbb{D}^4\mathbb{C}^3$ ; quadrature points:  $25 \times 25$  in a knot span  $\in \mathbb{R}^2$ ; solid line:  $\sigma_n^{(b)}$  and dashed line:  $\sigma_n^{(a)}$ .

knot span  $\in \mathbb{R}^2$  as a result of  $\mathbb{C}^0$ , where for dissimilar meshes between  $\Gamma_C^{(a)}$  and  $\Gamma_C^{(b)}$ , the projection can lead to unrealistic definition of quadrature quantities on  $\Gamma_C^{(b)}$ . But for higher-order continuity,  ${}^i w$  and  ${}^i J$  projected on a knot span  $\in \mathbb{R}^2$  are higher-order continuous across the knots and hence are distributed on the knot spans  $\in \mathbb{R}^2$  of the patch rather than to be confined within a knot span  $\in \mathbb{R}^2$  when the continuity is  $\mathbb{C}^0$  on the patch. Hence, the accuracy can be inferred to increase with increase in continuity. The accuracy associated with increase in the number of quadrature points can be explained as follows. As the number of quadrature points increase, the quadrature weight associated with a quadrature point decreases. Hence, for dissimilar meshes on  $\Gamma_C^{(a)}$  and  $\Gamma_C^{(b)}$ ,

lower the quadrature weights means lower the error in distribution of quadrature quantities across the knots in a given direction.

The effect of  $P$  on the accuracy of  $\sigma_n$  for the collocation method and the variational formulation is shown in Figure 10, considering  $\mathbb{D}^2\mathbb{C}^1$  parameterization. In addition with Greville points, the collocation scheme is also considered with equally spaced grid points in the parametric space over the patch. The total number of grid points is defined to be 81, and the total number of Greville points is 25 resulting from the NURBS parameterization. Meanwhile, the variational formulation was considered with  $12 \times 12$  number of Gauss points in a knot span  $\in \mathbb{R}^2$ . It is evident that the variational formulation yields less oscillation of  $\sigma_n$  for



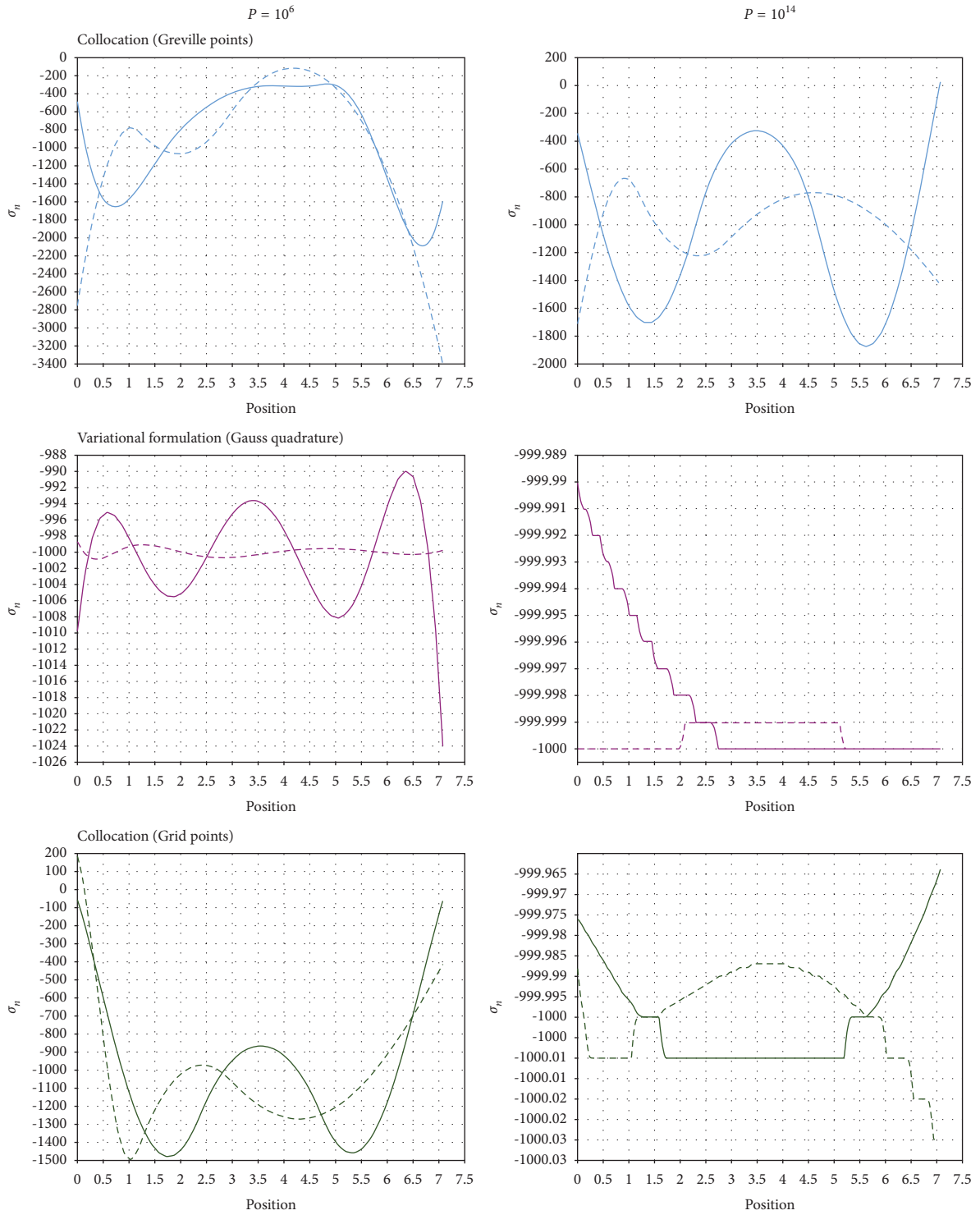


FIGURE 10: NURBS parameterization:  $\mathbb{D}^2\mathbb{C}^1$ ; quadrature points:  $15 \times 15$  in a knot span  $\in \mathbb{R}^2$ ; grid points:  $9 \times 9$  equally spaced points on  $\Gamma_C^{(p)}$  in parametric space; solid line:  $\sigma_n^{(b)}$  and dashed line:  $\sigma_n^{(a)}$ .

both the extremes of  $P$ , where for  $P = 10^6$  and  $P = 10^{14}$ , the differences in oscillation are  $\approx 34 \text{ N/m}^2$  and  $\approx 0.01 \text{ N/m}^2$ , respectively. While for the collocation method with the grid points, the difference in oscillation for  $P = 10^6$  is  $\approx 1700 \text{ N/m}^2$  which reduced drastically for  $P = 10^{14}$  to be  $\approx 0.06 \text{ N/m}^2$ . Collocation with the Greville points has the

worst oscillation for both the extremes of  $P$ , where for  $P = 10^6$  and  $P = 10^{14}$ , the differences in oscillation are  $\approx 3200 \text{ N/m}^2$  and  $\approx 1800 \text{ N/m}^2$ , respectively. This is likely since the accuracy of the collocation scheme with Greville points is known to be highly biased depending on the choice of surface considered for collocation [21]. To illustrate this,

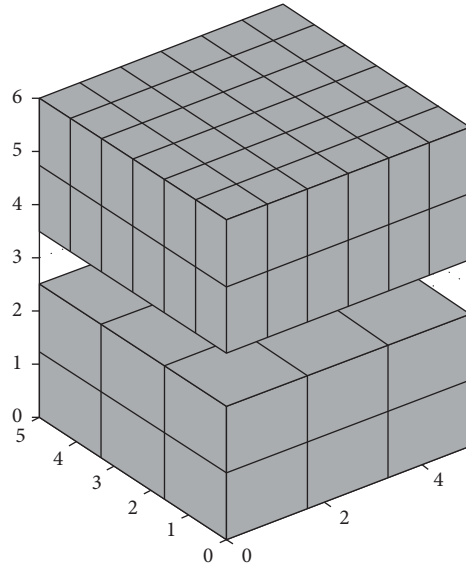


FIGURE 11: Contact patch test-2. Everything is the same as detailed in Figure 2 except for the NURBS parametrization shown here.

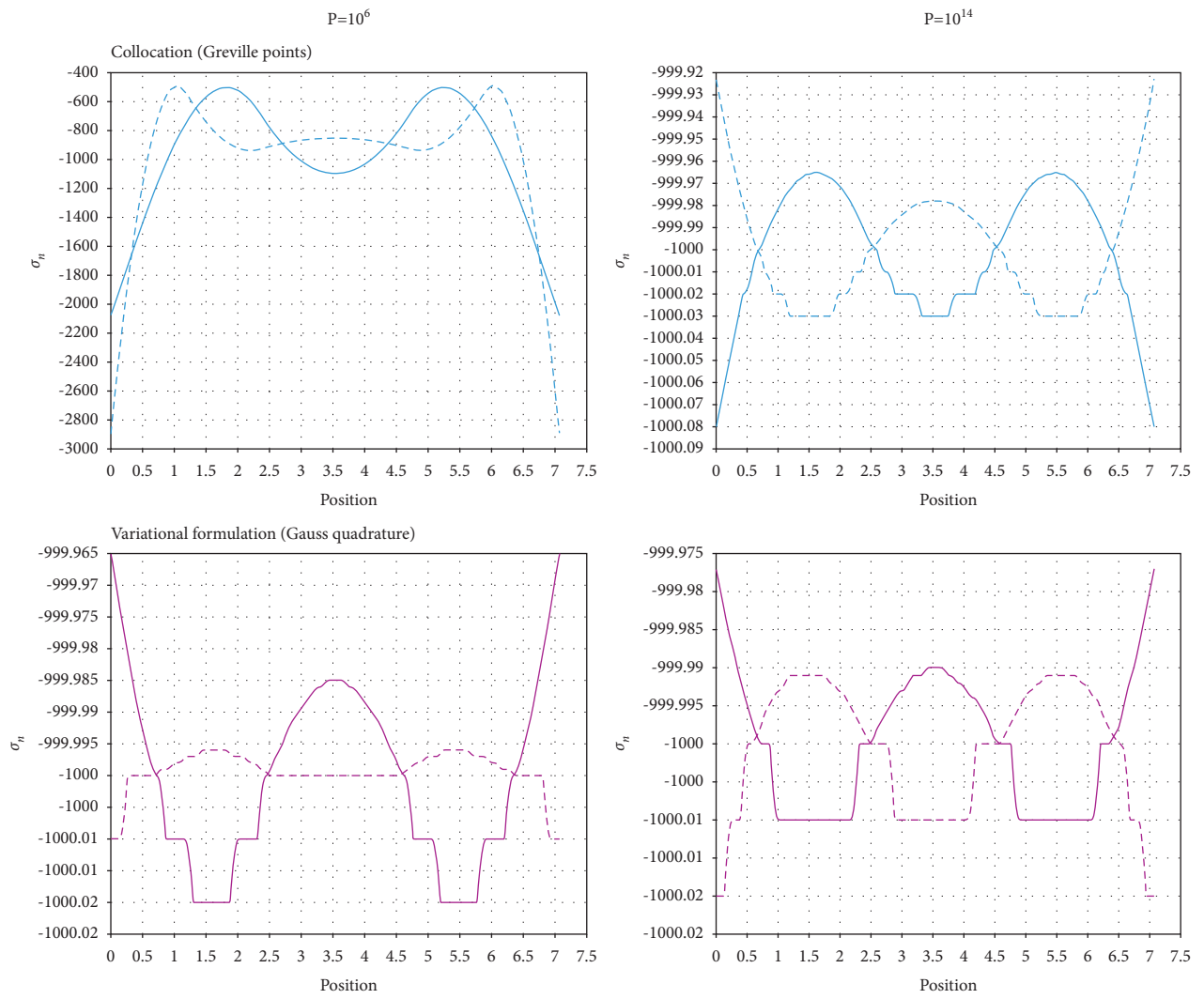
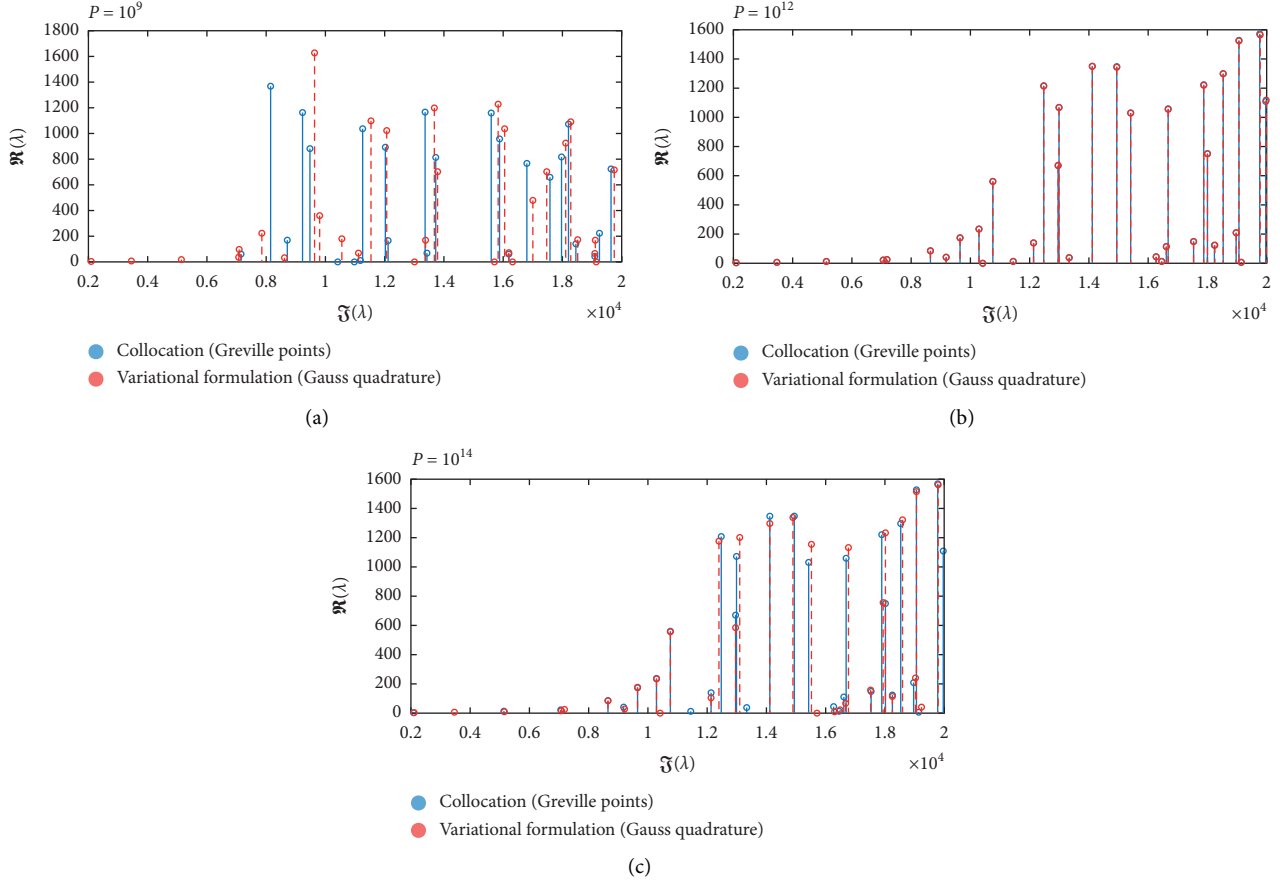


FIGURE 12: Results from contact patch test-2. NURBS parameterization:  $\mathbb{D}^2\mathbb{C}^1$ ; quadrature points:  $15 \times 15$  in a knot span  $\in \mathbb{R}^2$ ; solid line:  $\sigma_n^{(b)}$  and dashed line:  $\sigma_n^{(a)}$ .

FIGURE 13: Comparison of CEA results. NURBS parameterization:  $\mathbb{D}^2\mathbb{C}^1$ .

we consider a new parameterization as shown in Figure 11 for contact patch test 2. The results are shown in Figure 12 for the collocation method with Greville points and the variational formulation with the same setting as the preceding analysis. Considerable improvement for  $P = 10^{14}$  can be observed with collocation of the Greville points, where the difference in oscillation is  $\approx 0.16 N/m^2$  in comparison to  $\approx 0.05 N/m^2$  for the variational formulation. Nevertheless, still for  $P = 10^6$ , the difference in oscillation is  $\approx 2300 N/m^2$  in comparison to  $\approx 0.055 N/m^2$  with the variational formulation. For the case of a static analysis with contact, for which the contact constraint is satisfied with the penalty approach, given the proper choice of surface considered for collocation, collocation scheme with Greville points could be a good choice and more computationally efficient. But for accuracy at low values of  $P$  from the view point of the normal compliance approach, the variational formulation is more robust and the accuracy of  $\sigma_n$  is less sensitive to  $P$  and the choice of surface. The bias in the choice of surface for collocation could be overcome by the two-pass formulation though its numerical properties mainly in the context of CEA are not considered in this study. The oscillation of  $\sigma_n$  can indeed have an effect on steady-sliding equilibrium and the estimation of  $p(\mathbf{X})$  and  $\Gamma_C$  for linearization around the equilibrium, for which the variational formulation could be highly efficient in comparison with the collocation method.

With various formulations in approximating the integrals defined over  $\Gamma_C$ , the only difference is the relative variation of  $p(\mathbf{X})$  on  $\Gamma_C$  for a given  $P$ . The relative variation of  $p(\mathbf{X})$  infers the variation of  $\sigma_n$  owing to the inaccuracies in the approximation of the integrals defined over  $\Gamma_C$ , as observed with the contact patch test. Hence, the sensitivity of CEA for oscillations in  $\sigma_n$  can be inferred through comparing the collocation method and the variational formulation, which show different characteristics of oscillation for  $\sigma_n$  depending on  $P$ . Figure 13 shows comparison of CEA results for various values of  $P$  with the collocation method achieved through Greville points and the variational formulation. For collocation with Greville points, proper choice of contact surface is considered as inferred from the preceding discussion. It can be observed that for  $P = 10^9$ , the natural frequencies  $\Im(\lambda)$  and their corresponding instabilities  $\Re(\lambda)$  do not coincide between the formulations. The collocation method relatively seems to overestimate the instabilities  $\Re(\lambda)$  for  $\Im(\lambda) < 10\text{KHz}$ . For  $P = 10^{12}$ ,  $\Im(\lambda)$  and  $\Re(\lambda)$  are identical. Surprisingly, for  $P = 10^{14}$ , the results are largely identical but still not as identical as  $P = 10^{12}$ . We hypothesize this to be as a result of the increasing condition number of the matrices which shows the extremum of  $P$  considered. This indeed resembles the static case of the contact patch test in Figure 12 where for a large value of  $P$ , the accuracy of  $\sigma_n$  is nearly identical for the collocation

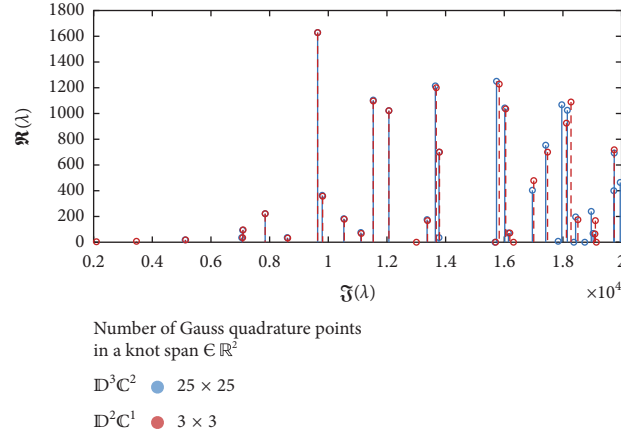
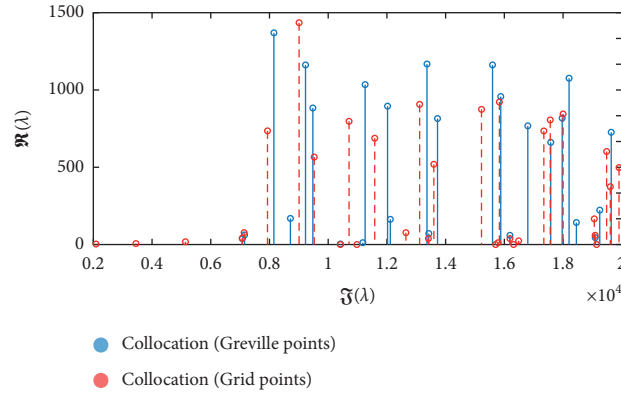


FIGURE 14: Comparison of CEA results.

FIGURE 15: Comparison of CEA results.  $P = 10^9$ ; NURBS parameterization:  $\mathbb{D}^2\mathbb{C}^1$ ; grid points:  $10 \times 10$  equally spaced points on  $\Gamma_C^{(p)}$  in parametric space.

method and the variational formulation. One can hypothesize from the patch test that the approximation error which is profound at lower values of  $P$  is implied through the oscillation of  $\sigma_n$  and consequently also has an effect on CEA. In contrast, at high values of  $P$ , CEA is less sensitive to the approximation error similar to the patch test, even with the collocation method which only models concentrated points of force. This means that for low values of  $p$ , the dynamics of the system are much sensitive to the relative variation of  $p(\mathbf{X})$  on  $\Gamma_C$ , which implies that characterizing the contact interface with global contact stiffness  $P$  may not be realistic with smaller values of local contact stiffness  $p(\mathbf{X})$ .

Despite the lack of the numerical benchmark to compare the results of CEA, the variational formulation can be considered to be the most accurate notably at low values of  $P$ , inferring from the results of the contact patch test. For the static analysis of the contact patch test, considerable improvement in the accuracy of  $\sigma_n$  was achieved with increasing the continuity and the number of Gauss quadrature points. This property could be useful if CEA is highly sensitive to the error in the discretization of  $p(\mathbf{X})$ . This is verified in Figure 14 where no considerable variation could be observed except for small shift in frequencies at high frequencies,  $\Im(\lambda) > 13\text{KHz}$ , which could be as a result

of convergence. Hence, it can be inferred that at low values of  $P$ , CEA is not sensitive to the scale of improvement in the accuracy of approximation provided by increasing the continuity or the number of Gauss quadrature points for the variational formulation, but it is certainly sensitive to the scale of improvement in the accuracy of approximation between the collocation and the variational formulation. To further show the sensitivity of collocation, we compare the collocation method between nearly identical number of grid points and Greville points. The number of equally spaced grid points in the parametric space was defined to be 100 for the 104 Greville points inferred from the NURBS parameterization. In this case, the only difference is the positions in which the collocation is defined. The comparison is shown in Figure 15, where the results are observed to be different.

#### 4. Conclusion

Numerically, the results imply that for low values of contact stiffness, the dynamical response is sensitive to the relative variation of contact stiffness at the interface. This factor proves to be sensitive with approximations in defining a contact formulation. We show that the defined collocation method is inaccurate at low contact stiffness and hence can

be largely deemed to be inefficient with the normal compliance approach. Even though the collocation formulation was defined from the variational formulation, the analogy of modelling concentrated points of force can be in general extended to other collocation-type formulations and hence also the inaccuracy associated with it. This is also true in classical finite element analysis with methods such as node-to-node and node-to-surface formulations. While for large values of contact stiffness, the dynamics is less sensitive to the relative variation of contact stiffness and converges with increase in contact stiffness. Hence, to satisfy Signorini conditions with the penalty approach where the penalty value can be interpreted as high contact stiffness, the collocation method can be accurate with the right choice of collocation points and a collocation surface for the half-pass formulation. For computational efficiency while preserving good accuracy, collocation points based on NURBS parameterization such as points defined with Greville abscissae which in general implies few number of collocation points can be even efficient.

For the normal compliance approach, notably at low contact stiffness, preserving the integral nature of the variational formulation, even approximately without domain decomposition proves to be efficient and robust. We show that CEA could be analyzed robustly and accurately with the accuracy of such formulations. The inference from the results realized with the isogeometric approach can also be extended to classical finite element methods, except for the higher-continuity of the spline basis functions can be more accurate than with the classical finite element  $c^0$  basis functions. Such comparisons have been largely discussed in the literature. We also showed that the contact patch test cannot be relied to imply accuracy for CEA, where we referred to a lumped approach which is superior in the patch test, proving to be numerically unstable for CEA.

## Data Availability

The data used to support the findings of this study are included within the article.

## Conflicts of Interest

The authors declare that they have no conflicts of interest.

## References

- [1] A. Akay, "Acoustics of friction," *Journal of the Acoustical Society of America*, vol. 111, no. 4, pp. 1525–1548, 2002.
- [2] R. A. Ibrahim, "Friction-induced vibration, chatter, squeal, and chaos—Part I: mechanics of contact and friction," *Applied Mechanics Reviews*, vol. 47, no. 7, pp. 209–226, 1994.
- [3] R. A. Ibrahim, "Friction-induced vibration, chatter, squeal, and chaos—Part II: dynamics and modeling," *Applied Mechanics Reviews*, vol. 47, no. 7, pp. 227–253, 1994.
- [4] N. Kinkaid, O. M. O'Reilly, and P. Papadopoulos, "Automotive disc brake squeal," *Journal of Sound and Vibration*, vol. 267, no. 1, pp. 105–166, 2003.
- [5] K. Soobarayen, J.-J. Sinou, and S. Besset, "Numerical study of friction-induced instability and acoustic radiation-effect of ramp loading on the squeal propensity for a simplified brake model," *Journal of Sound and Vibration*, vol. 333, no. 21, pp. 5475–5493, 2014.
- [6] M. R. North, *Disc Brake Squeal: A Theoretical Model*, MIRA Noneaton, England, UK, 1972.
- [7] J. T. Oden and J. A. C. Martins, "Models and computational methods for dynamic friction phenomena," *Computer Methods in Applied Mechanics and Engineering*, vol. 52, no. 1-3, pp. 527–634, 1985.
- [8] D. Bigoni and G. Noselli, "Experimental evidence of flutter and divergence instabilities induced by dry friction," *Journal of the Mechanics and Physics of Solids*, vol. 59, pp. 2208–2226, 2011.
- [9] H. Ouyang, W. Nack, Y. Yuan, and F. Chen, "Numerical analysis of automotive disc brake squeal: a review," *International Journal of Vehicle Noise and Vibration*, vol. 1, no. 3/4, pp. 207–231, 2005.
- [10] Q. Nguyen and F. Moirrot, "Brake squeal: a problem of flutter instability of the steady sliding solution?" *Archives of Mechanics*, vol. 4, pp. 645–662, 2000.
- [11] J. A. C. Martins, S. Barbarin, M. Raous, and A. Pinto da Costa, "Dynamic stability of finite dimensional linearly elastic systems with unilateral contact and Coulomb friction," *Computer Methods in Applied Mechanics and Engineering*, vol. 177, no. 3-4, pp. 289–328, 1999.
- [12] J. J. Sinou and L. Jézéquel, "Mode coupling instability in friction-induced vibrations and its dependency on system parameters including damping," *European Journal of Mechanics-A: Solids*, vol. 26, no. 1, pp. 106–122, 2007.
- [13] K. A. Fischer and P. Wriggers, "Frictionless 2d contact formulations for finite deformations based on the mortar method," *Computational Mechanics*, vol. 36, no. 3, pp. 226–244, 2005.
- [14] K. A. Fischer and P. Wriggers, "Mortar based frictional contact formulation for higher order interpolations using the moving friction cone," *Computer Methods in Applied Mechanics and Engineering*, vol. 195, no. 37-40, pp. 5020–5036, 2006.
- [15] B. Yang, T. Laursen, and X. Meng, "Two dimensional mortar contact methods for large deformation frictional sliding," *International Journal for Numerical Methods in Engineering*, vol. 62, no. 9, pp. 1183–1225, 2005.
- [16] A. Klarbring, A. Mikelić, and M. Shillor, "Frictional contact problems with normal compliance," *International Journal of Engineering Science*, vol. 26, no. 8, pp. 811–832, 1988.
- [17] T. J. R. Hughes, J. A. Cottrell, and Y. Bazilevs, "Isogeometric analysis: cad, finite elements, nurbs, exact geometry and mesh refinement," *Computer Methods in Applied Mechanics and Engineering*, vol. 194, no. 39-41, pp. 4135–4195, 2005.
- [18] J. A. Cottrell, A. Reali, Y. Bazilevs, and T. J. R. Hughes, "Isogeometric analysis of structural vibrations," *Computer Methods in Applied Mechanics and Engineering*, vol. 195, no. 41-43, pp. 5257–5296, 2006.
- [19] L. De Lorenzis, P. Wriggers, and T. J. Hughes, "Isogeometric contact: a review," *GAMM-mitteilungen*, vol. 37, no. 1, pp. 85–123, 2014.
- [20] İ. Temizer, P. Wriggers, and T. Hughes, "Contact treatment in isogeometric analysis with nurbs," *Computer Methods in Applied Mechanics and Engineering*, vol. 200, no. 9-12, pp. 1100–1112, 2011.
- [21] M. E. Matzen, T. Cichosz, and M. Bischoff, "A point to segment contact formulation for isogeometric, nurbs based finite elements," *Computer Methods in Applied Mechanics and Engineering*, vol. 255, pp. 27–39, 2013.

- [22] E. Brivadis, A. Buffa, B. Wohlmuth, and L. Wunderlich, "Isogeometric mortar methods," *Computer Methods in Applied Mechanics and Engineering*, vol. 284, pp. 292–319, 2015.
- [23] P. Wriggers, "Finite element algorithms for contact problems," *Archives of Computational Methods in Engineering*, vol. 2, no. 4, pp. 1–49, 1995.
- [24] P. Mohanasundaram, G. Frédéric, S. Besset, and K. Shimoyama, "Multi-references acquisition strategy for shape optimization of disc-pad-like mechanical systems," *Structural and Multidisciplinary Optimization*, vol. 64, p. 10, 2021.
- [25] K. Shintani and H. Azegami, "Shape optimization for suppressing brake squeal," *Structural and Multidisciplinary Optimization*, vol. 50, no. 6, pp. 1127–1135, 2014.
- [26] G. Duvaut and J. L. Lions, *Inequalities in Mechanics and Physics. Grundlehren der mathematischen Wissenschaften in Einzeldarstellungen mit besonderer Berücksichtigung der Anwendungsgebiete*, Springer-Verlag, Berlin, Germany, 1976.
- [27] J. A. C. Martins and J. T. Oden, "Existence and uniqueness results for dynamic contact problems with nonlinear normal and friction interface laws," *Nonlinear Analysis: Theory, Methods & Applications*, vol. 11, no. 3, pp. 407–428, 1987.
- [28] J. J. Moreau and P. D. Panagiotopoulos, *Unilateral Contact and Dry Friction in Finite Freedom Dynamics*, Springer Vienna, Vienna, Austria, 1988.
- [29] P. Rabier, J. A. C. Martins, J. T. Oden, and L. Campos, "Existence and local uniqueness of solutions to contact problems in elasticity with nonlinear friction laws," *International Journal of Engineering Science*, vol. 24, no. 11, pp. 1755–1768, 1986.
- [30] M. E. Matzen and M. Bischoff, "A weighted point-based formulation for isogeometric contact," *Computer Methods in Applied Mechanics and Engineering*, vol. 308, pp. 73–95, 2016.
- [31] P. Papadopoulos, R. E. Jones, and J. M. Solberg, "A novel finite element formulation for frictionless contact problems," *International Journal for Numerical Methods in Engineering*, vol. 38, no. 15, pp. 2603–2617, 1995.
- [32] R. A. Sauer and L. De Lorenzis, "A computational contact formulation based on surface potentials," *Computer Methods in Applied Mechanics and Engineering*, vol. 253, pp. 369–395, 2013.
- [33] N. Elabbasi and K. J. Bathe, "Stability and patch test performance of contact discretizations and a new solution algorithm," *Computers & Structures*, vol. 79, no. 16, pp. 1473–1486, 2001.
- [34] T. X. Duong and R. A. Sauer, "An accurate quadrature technique for the contact boundary in 3d finite element computations," *Computational Mechanics*, vol. 55, no. 1, pp. 145–166, 2015.
- [35] D. Schillinger, L. Dede, M. A. Scott et al., "An isogeometric design-through-analysis methodology based on adaptive hierarchical refinement of nurbs, immersed boundary methods, and t-spline cad surfaces," *Computer Methods in Applied Mechanics and Engineering*, vol. 249–252, pp. 116–150, 2012.
- [36] C. Giannelli, B. Jüttler, S. K. Kleiss, A. Mantzaflaris, B. Simeon, and J. Špeh, "Thb-splines: an effective mathematical technology for adaptive refinement in geometric design and isogeometric analysis," *Computer Methods in Applied Mechanics and Engineering*, vol. 299, pp. 337–365, 2016.
- [37] D. Tonazzi, F. Massi, M. Salipante, L. Baillet, and Y. Berthier, "Estimation of the normal contact stiffness for frictional interface in sticking and sliding conditions," *Lubricants*, vol. 7, no. 7, p. 56, 2019.